radioresistance with the activation of the AKT/cyclin D1 pathway following irradiation, but this activation was not observed in corresponding parental cells. Radioresistance of CSCs was suppressed by combination of 2 Gy of FR and reagents such as an AKT inhibitor of AKT/PKB signaling pathway (API-2) and a Cdk4 inhibitor. Thus, we have demonstrated that AKT, cylin D1 and Cdk4 are important molecular targets to suppress radioresistance of CSCs.

RESULTS

Isolation of CD133-positive CSCs by long-term FR

In order to isolate radioresistant tumor cells against long-term FR, HepG2 and A172 cells were exposed to FR with 0.5 Gy of X-rays every 12 h for up to 82 days. A dramatic increase in the level of CD133, a marker of CSCs[18] was observed after FR for 82 days in all cell lines examined, but was not in cells exposed for 14 days (14FR cells) and 31 days (31FR cells) (Figure 1a). We have previously reported that 31FR cells have acquired radioresistance by exposure to FR for 31 days.[16] 31FR cells with acquired radioresistance are not equal to CSCs because they were negative for CD133 (Figure 1a). We next measured the ratio of CD133-positive cells by fluorescence-activated cell sorting (FACS) with phycoerythrin-conjugated anti-CD133 antibody in 82FR cells after the cessation of FR for over 1 month (hereafter referred to as 82FR-31 non-radiation (82FR-31NR) cells) (Figure 1b). CD133-positive cells were $<10\%$ before FR, but increased to around 90% in 82FR-31NR cells in both cell lines (Figure 1c).

CD133-positive cells were likely to be enriched by selectively killing radiosensitive CD133-negative cells by FR. In order to examine this possibility, CD133 expression was investigated in the colony that survived against 5-Gy irradiation. The number of colonies made of CD133-positive cells apparently increased after 5-Gy irradiation to HepG2 (Figure 1d). This result indicated that CD133-negative cells are more sensitive to radiation than CD133-positive cells.

In order to characterize 82FR-31NR cells, we investigated mRNA expression of CD133, ABC transporters such as MDR1 (multi drug resistance 1) and BCRP1 (breast cancer resistance protein), albumin and GFAP (glial fibrillary acidic protein) by reverse transcription PCR in parental 0FR cells and 82FR-31NR cells (Figure 1e). As expected, CSC-related genes such as *CD133* and *BCRP1* were upregulated in 82FR-31NR cells compared with their parental cells in both cell lines. MDR1 expression is also higher in A172 82FR-31NR cells than that in A172 0FR cells. Conversely, the astrocyte marker GFAP was downregulated in A172 82FR-31NR cells compared with A172 0FR cells.

We further examined protein expression of liver stem cell marker cytokeratin14 in HepG2 cells by immunostaining. In contrast to parental 0FR cells, cytokeratin14 positive cells were observed in 82FR-31NR HepG2 (Figure 1f).

Using xenotransplntation into nude mice, we next confirmed tumorigenic potential of parental 0FR cells and 82FR-31NR cells from HepG2 and A172. Tumorigenic incidence was higher in 82FR-31NR cells than in parental 0FR cells (Table 1). These results demonstrated that exposure to FR for 82 days enriched CSCs owing to their radioresistance compared with non-stem cells.

Radioresistance of 82FR-31NR cells

We analyzed colony survival of 82FR-31NR cells after 2, 5 and 10-Gy irradiation. Compared with corresponding parental 0FR cells, significant radioresistance was observed at all the doses in 82 FR-31NR cells of both cell lines (Figure 2a). Fraction of annexin V positive apoptoic cells increased after 5-Gy irradiation in parental

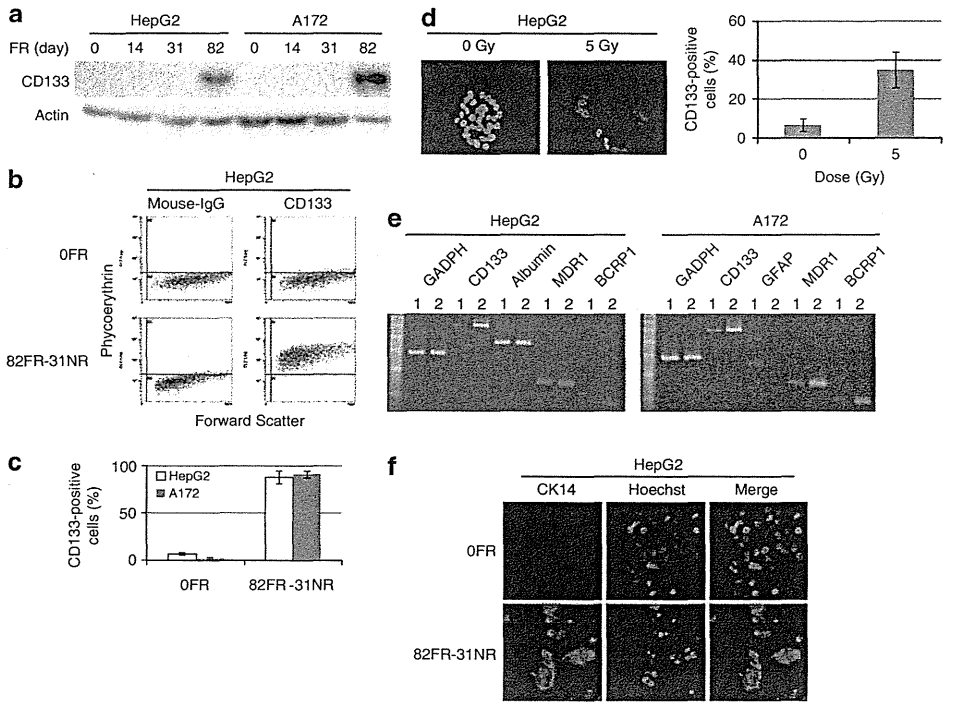

Figure 1. Isolation of CD133-positive cells by radiation exposure. (**a**) Western blotting of CD133 and β-actin in HepG2 and A172 cells at the indicated day of FR. (**b**) FACS analysis of CD133-positive cells by using phycoerythrin-conjugated anti-CD133 antibodies. Phycoerythrin-conjugated mouse-IgG antibody is used as negative control. (**c**) The percentage of CD133-positive cells was determined by FACS analysis as shown in **b**. (**d**) CD133 positive cells in the colony of HepG2. The colony was made by incubating irradiated cells for 6 days and then immunofluorescence was performed. The percentage of the colony consisting of CD133-positive cells was shown on the right graph. (**e**) mRNA expression of *GADPH, CD133, Albumin, MDR1, GFAP* and *BCRP1* in parental 0FR cells (lane 1) and 82FR-31NR cells (lane 2). *GADPH* was used for internal control. (**f**) Immunofluorescence staining with cytokeratin14 in 0FR and 82FR-31NR cells of HepG2. Nuclei were stained with Hoechst.

Table 1. Tumor incidence in nude mice

Cells	*No. of tumors/no. of mice injected*	
	With 5 × 10^5 cells	*Tumor incidence*
HepG2	2/9	22.2
HepG2 82FR-31NR	12/15	80.0
A172	0/6	0
A172 82FR-31NR	7/9	77.8

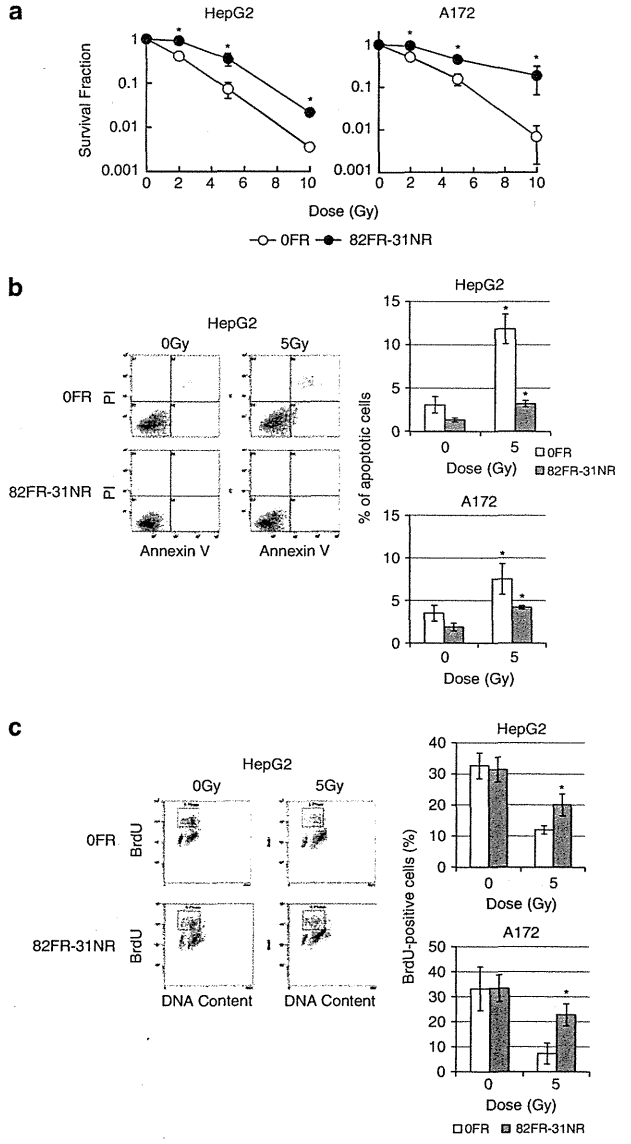

Figure 2. Radioresistance of 82FR-31NR cells. (**a**) Survival curves of 0FR (open circle) and 82FR-31NR cells (closed circle) of HepG2 on the left and those of A172 on the right, after irradiation. Asterisks indicate significant radioresistance in 82FR-31NR cells as compared with 0FR cells. (**b**) Annexin V staining in 0FR and 31FR-31NR cells. Asterisks indicate significant increase of apoptotic cells by irradiation in 0FR and 82FR-31NR cells in comparison with non-irradiated cells. (**c**) The growth recovery after irradiation. Percentage of BrdU-positive cells was shown in right graph. FACS analysis was done on cells 25 h after 5-Gy irradiation. Asterisks indicate significant increase of BrdU-positive cells in 82FR-31NR cells with 5 Gy in comparison with 0FR cells with 5-Gy irradiation.

0FR cells, whereas apoptosis was less induced in 82FR-31NR cells in both cell lines (Figure 2b).

In order to analyze the growth recovery after radiation exposure, cells were irradiated with 5-Gy X-rays and were cultured for 24 h, pulse-labeled with BrdU (bromodeoxyuridine) for 1 h, and subjected to FACS analysis (Figure 2c). Exposure to 5 Gy decreased BrdU-positive cells in parental 0FR cells and 82FR-31NR cells in both cell lines, but the percentage of BrdU-positive cells was higher in 82FR-31NR cells than in parental 0FR cells 25 h after 5-Gy irradiation. This result showed that 82FR-31NR cells more proliferated than parental 0FR cells after irradiation.

Radiation-induced activation of the AKT/cyclin D1 pathway for efficient DNA repair in 82FR-31NR cells

We studied DDR of 82FR-31NR cells to elucidate the molecular mechanisms underlying radioresistance of CSCs. We examined kinase activity of AKT in HepG2 parental 0FR cells and HepG2 82FR-31NR cells by determining phosphorylation at Serine473 (P-AKT Ser473) after irradiation (Figure 3a). Exposure to 5-Gy X-rays significantly induced apoptosis in parental 0FR cells, but not in 82FR-31NR cells (Figure 2b). AKT phosphorylation was observed 3 h after 5-Gy irradiation in 82FR-31NR cells and maintained for 24 h. However, AKT phosphorylation in parental 0FR cells was not increased at any time point examined after irradiation. The total AKT level in 82FR-31NR cells once decreased and then restored to the un-irradiated control level at 12 and 24 h after treatment, whereas the level tended to decrease in 0FR cells after irradiation. Cyclin D1, downstream of AKT pathway, was also upregulated following irradiation in 82FR-31NR cells with increased P-AKT Ser473 (Figure 3a). Conversely, cyclin D1 was degraded after DNA damage in parental 0FR cells.

We speculated that induction of apoptosis by 5-Gy irradiation in parental 0FR cells was caused by activation of the p53 pathway, which regulates pro-apoptotic genes. As expected, the expression of p53 increased by irradiation in parental 0FR cells, whereas this was not observed in 82FR-31NR cells (Figure 3a). Interestingly, p53 was completely negative in 82FR-31NR cells regardless of exposure to acute radiation. Loss of p53 may associate with enrichment of CSCs induced by long-term FR.

We further examined correlation between AKT activation and DNA repair in 82FR-31NR cells. The repair kinetics of double strand breaks was examined by western blotting of γ-H2AX.[19,20] γ-H2AX was first detected 30 min after exposure to 5-Gy X-rays in 0FR and 82FR-31NR cells. The γ-H2AX level was restored to untreated control level (1.0) at 6 h after irradiation in 82FR-31NR cells, whereas the level still indicated > 1.0 at that time in parental 0FR cells of both cell lines (Figure 3b). This efficient DNA repair in 82FR-31NR cells represented the nature of CSC. Upon treatment with API-2 or cyclin D1 siRNA, disappearance of γ-H2AX signal was suppressed and the γ-H2AX level was > 1.0 at 6 h after irradiation in 82FR-31NR cells of both cell lines (Figures 3c and d). Thus, AKT/cyclin D1 pathway was associated with efficient DNA repair in 82FR-31NR cells after radiation.

Suppression of radioresistance in 82FR-31NR cells by inhibiting the AKT/cyclin D1 pathway

We studied the role of the AKT pathway in radioresistance of 82FR-31NR cells. We examined whether inhibiting the AKT/cyclin D1 pathway suppressed radioresistance of 82FR-31NR cells or not. We used API-2, rapamycin and a Cdk4 inhibitor (Cdk4-I), which suppresses the activity of cyclin D1/Cdk4. API-2 attenuated phosphorylation of AKT at Ser473 in 0FR and 82FR-31NR cells of HepG2. Rapamycin attenuated phosphorylation of downstream targets of mTOR including p70S6K and S6 in 0FR and 82FR-31NR cells of HepG2 (Figure 4a). We previously reported that 1.9 μM of Cdk4-I can suppress the kinase activity of cyclin D1/Cdk4 in HepG2 cells.[16]

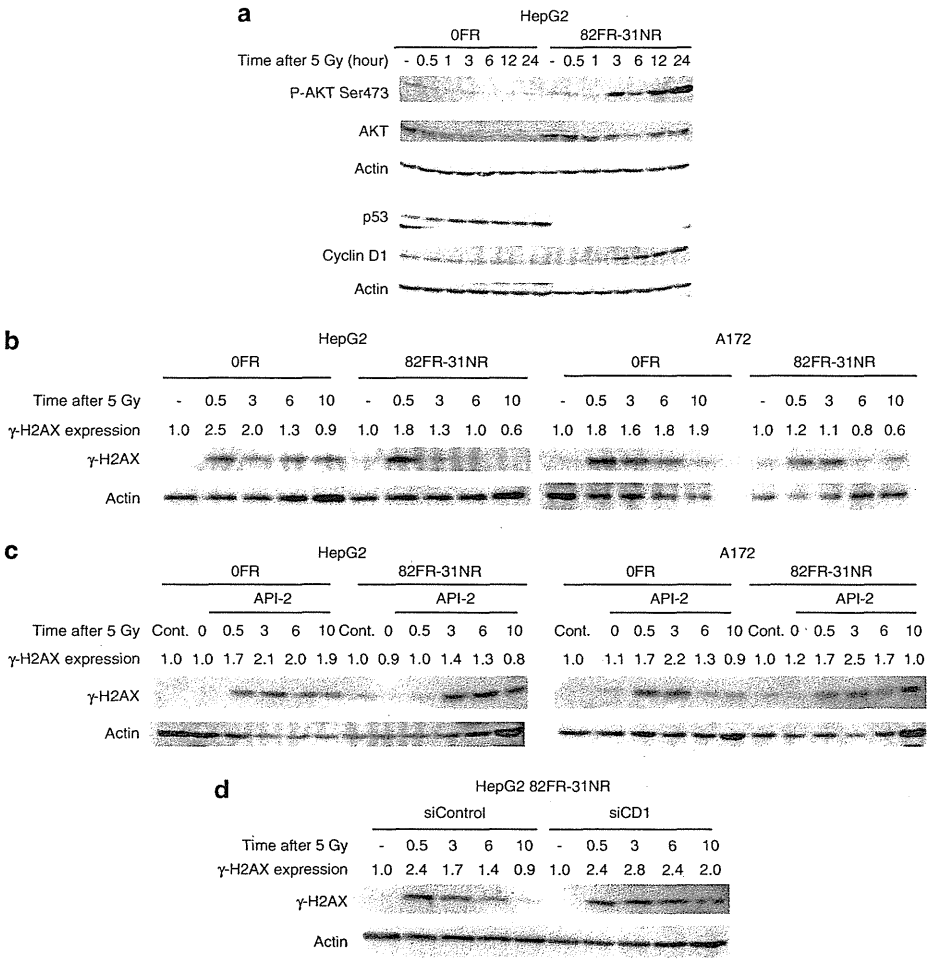

Figure 3. Activation of the AKT/cyclin D1 pathway for efficient DNA repair in 82FR-31NR cells. (**a**) Western blotting of phosphorylated-AKT-Serine 473 (P-AKT Ser473), AKT, p53, cyclin D1 and β-actin in 0FR and 82FR-31NR cells. (**b**) Western blotting of γ-H2AX and β-actin in 0FR and 82FR-31NR cells of HepG2 and A172 after 5-Gy irradiation at indicated time points. (**c**) Western blotting of γ-H2AX and β-actin in 0FR and 82FR-31NR cells of HepG2 and A172 with radiation plus API-2. Cells were treated with 20 μM of API-2 for 24 h and then the drug was removed by washing out before irradiation. (**d**) Western blotting of γ-H2AX and β-actin in 0FR and 82FR-31NR cells of HepG2 and A172 by control siRNA (siControl) and cyclin D1 siRNA (siCD1) was shown. The amounts of γ-H2AX were normalized by corresponding β-actin level. The values are expressed relative to the untreated control value.

Treatment with API-2 or Cdk4-I rendered 82FR-31NR cells of HepG2 and A172 susceptibility to radiation, whereas rapamycin had no effect on the radiosensitivity of those cells (Figure 4b). Apoptosis was examined by annexin V staining in 82FR-31NR cells of HepG2 and A172 (Figure 4c). Annexin V positive apoptosis was induced by treatment with API-2 or Cdk4-I in 82FR-31NR cells, except in A172 83FR-31NR with rapamycin. Incidence of apoptosis was further increased by the combination of radiation and API-2 or Cdk4-I in 82FR-31NR cells in both cell lines, whereas the incidence of apoptosis was not affected by combination of radiation and rapamycin. These results demonstrated that the AKT/cyclin D1/Cdk4 pathway, but not the AKT/mTOR pathway, is responsible for radioresistance of 82FR-31NR cells.

In standard fractionated RT, multiple 2 Gy of FR was administrated to tumors. We investigated radiosensitivity to 2 Gy of FR in 82FR-31NR cells of HepG2 and A172 (Figures 4d and e). The growth of parental HepG2 and A172 cells was completely inhibited by 2 Gy of FR for 11 days.[17] Although the growth was retarded by FR in 82FR-31NR cells of HepG2 and A172, they can grow during exposure of 2 Gy of FR. This radioresistance of 82FR-31NR cells against 2 Gy of FR was suppressed by the combination with either API-2 or Cdk4-I (Figures 4d and e). Therefore, we assumed that the AKT, cyclin D1 and Cdk4 are feasible molecular targets for suppression of radioresistance of CSCs.

We further assessed the importance of cyclin D1 and Cdk4 in radioresistance of 82FR-31NR cells. The expression of these proteins was suppressed by cyclin D1 siRNA and Cdk4 siRNA, respectively (Figure 5a). Radioresistance of 82FR-31NR cells disappeared by downregulation of cyclin D1 or Cdk4 concomitant with increased radiation-induced apoptosis (Figures 5a and b). These results demonstrated that cyclin D1 and Cdk4 are important molecular targets for the suppression of radioresistance in CSCs.

DISCUSSION

Enrichment of CSCs by radiation exposure

Tumor control is commonly assessed by reduction of the main tumor mass for evaluation of the efficacy of cancer treatment. The drawback of this estimation is that tumor regression by cancer treatment dose not correlate well with the loss of tumorigenicity. One surviving CSC has potential to make recurrent tumors after treatments. Therefore, it is tremendously important to eradicate

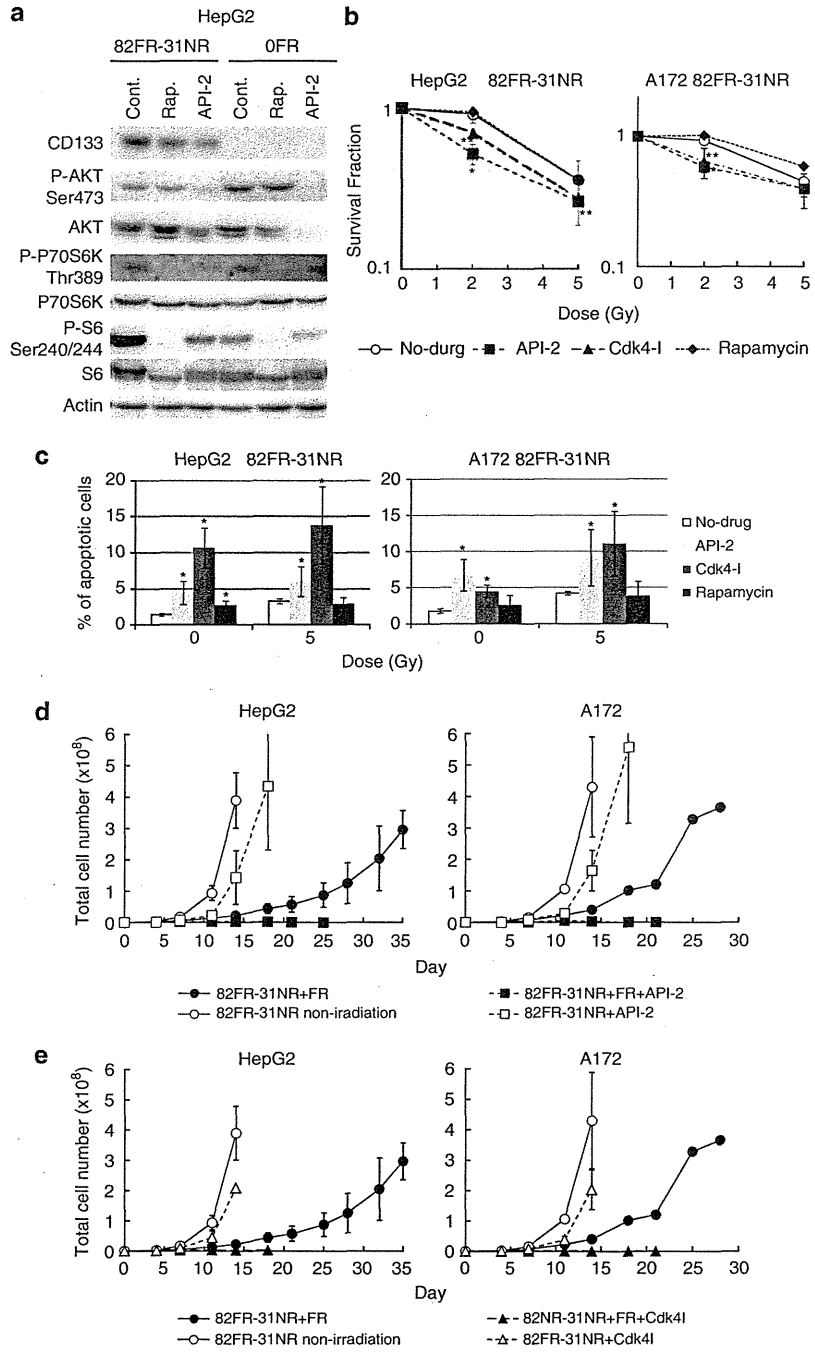

Figure 4. Targeting the AKT/cyclin D1/Cdk4 pathway for suppression of radioresistance of 82FR-31NR cells. (**a**) Western blotting of CD133, P-AKT Ser473, AKT, phosphorylated-p70S6K-Threonine389 (P-P70S6K-Thr389), P70S6K, phosphorylated-S6-Serine240/Serine244 (P-S6-Ser240/244), S6 and β-actin in 0FR and 82FR-31NR cells with rapamycin or API-2. (**b**) Survival curves of 82FR-31NR cells (open circle), 82FR-31NR cells with API-2 (closed square), 82FR-31NR cells with Cdk4-I (closed triangle), 82FR-31NR cells with rapamycin (closed diamond) of HepG2 on the left and those of A172 on the right, after irradiation. Asterisks indicate significant radioresistance in 82FR-31NR cells with each drug compared with 82FR-31NR cells without drug. (**c**) Annexin V staining in 82FR-31NR cells. Asterisks indicate significant increase of Annexin V positive cells by treatment with drugs in 82FR-31NR cells in comparison with non-treated cells. (**d**) Cell growth in 82FR-31NR cells with 2 Gy of FR (closed circle), 82FR-31NR with FR plus API-2 (closed square), non-irradiated 82FR-31NR cells (open circle) and 82FR-31NR with API-2 (open square). Cells were treated with 20 μM of API-2 for 24 h once a week. (**e**) Cell growth in 82FR-31NR cells with 2 Gy of FR (closed circle), 82FR-31NR with FR plus Cdk4-I (closed triangle), non-irradiated 82FR-31NR cells (open circle) and 82FR-31NR with Cdk4-I (open triangle). Cells were treated with 1.9 μM of the Cdk4-I for 24 h once a week.

CSCs completely for the cure of cancer.[7] Most CSC studies have utilized a magnetic-beads-conjugated anti-CD133 antibody to isolate CSCs in a heterogeneous population.[4] Other than this procedure, radiation and anti-cancer drug enrich radio- and chemo-resistant CSCs, which are implicated in treatment failures of RT or chemotherapy.[21–24]

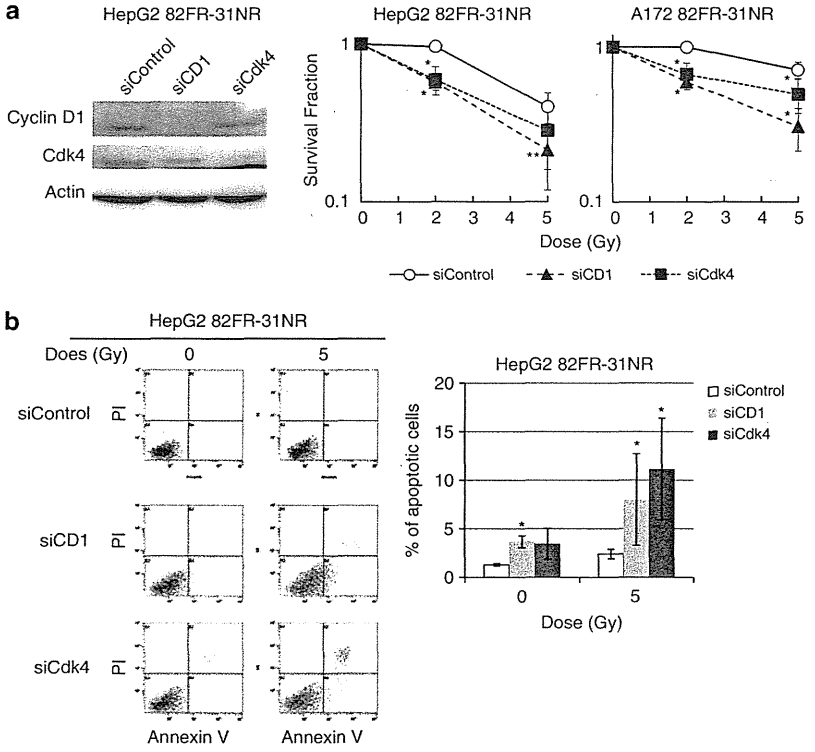

Figure 5. Suppression of radioresistance in 82FR-31NR cells by targeting cyclin D1/Cdk4. (**a**) Western blotting of cyclin D1, Cdk4 and β-actin by control siRNA (siControl), cyclin D1 siRNA (siCD1) and Cdk4 siRNA (siCdk4) are shown in the left panel. Western blotting was performed by using cell extracts collected 48 h after transfection. Survival curves of 82FR-31NR cells with siControl (open circle), siCD1 (closed triangle) or siCdk4 (closed square) after irradiation are shown. Cells were irradiated 24 h after transfection. Asterisks indicate significant radiosensitization in 82FR-31NR cells by siCD1 or siCdk4 compared with 82FR-31NR cells with siControl. (**b**) FACS analyses of apoptosis after 5-Gy irradiation on 82FR-31NR cells with siControl, siCD1 or siCdk4. Cells were irradiated 48 h after transfection and stained with Annexin V and propidium iodide. The percentages of apoptotic cells are shown on the right graph. Asterisk indicates that siCD1 or siCdk4 significantly induced apoptosis in 82FR-31NR cells compared with siControl.

In this study, we have isolated surviving CSCs against FR by exposure to relatively low-dose X-rays for 82 days. We consider that our established 82FR-31NR cells are CSCs because they showed higher expression of CD133 and ABC transporters, high tumorigenic potential, radioresistance, and efficient DNA repair of radiation-induced DNA damage compared with their parental cell lines. CSCs were selected after exposure to FR for over two months and cultured *in vitro* for a long time, and the possibility remains that they are different from CSCs directly isolated from primary tumors. However, CSCs in the present study fulfilled the characteristics as CSCs. Isolation of CSC fraction by radiation was due to the selection of radioresistant CSCs or mutations toward the acquisition of the ability to self-renew in non-stem cells. Our data of preferential survival of CD133-positive cells against radiation damage indicated that radiation has an ability to enrich CSCs by selectively killing radiosensitive non-stem cells in an *in vitro* heterogeneous population.

Activation of the AKT/cyclin D1 pathway by radiation exposure in 82FR-31NR cells

Several internal cell signaling pathways, including the PI3K/AKT pathway, are activated by the serum-free culture condition specific to CSCs containing epidermal growth factor and basic fibroblast growth factor. These activations are not seen in the growth medium of monolayer cells.[8] Both growth factors have previously been shown to decrease cellular radiosensitivity.[25,26] Therefore, it would be better to compare cells and their derived CSCs under the same culture condition for seeking for molecular targets of CSC treatments. Our isolated 82FR-31NR cells have an ability to self-renew even in the medium containing serum. Thus, we can analyze DDR of CSCs in as the same growth medium as that of parental cells

According to FACS analysis and western blotting data of 82FR-31NR cells, those cells can grow after irradiation with the activation of the AKT/cyclin D1 survival signaling pathway. In contrast, parental cells died after the same dose of irradiation without activation of the AKT pathway.

DDR regarding the AKT/cyclin D1 pathway in response to radiation is depicted in Figure 6. In parental cells, radiation-induced DNA damage activated p53, which promotes apoptosis in irradiated cells. In contrast, the AKT/cyclin D1/Cdk4 pathway was activated in 82FR-31NR cells by irradiation. Radiation-induced DNA damage was efficiently repaired in 82FR-31NR cells. Thus, the AKT/cyclin D1 pathway is a key to facilitate DNA repair of 82FR-31NR cells after irradiation. As reported previously, the PI3K/AKT pathway is implicated in DNA repair of radiation-induced DNA damage in glioma cells.[27] Cyclin D1 regulates not only cell cycling, but also enhances DDR of homologous recombination repair (HRR) in cooperation with Rad51.[28] We have previously reported that cyclin D1 knockdown by its siRNA decreases homologous recombination repair activity in radioresistant cells.[16] Collectively, these observations indicate that cyclin D1 is a potent target to increase radiosensitivity of radioresistant cells by inhibiting homologous recombination repair. Indeed, DNA repair was impeded in 82FR-31NR cells by inhibiting the AKT/cyclin D1

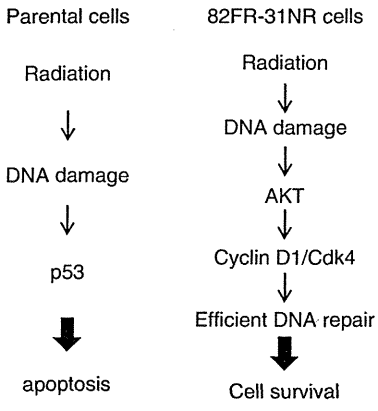

Figure 6. DNA damage signaling pathway in parental cells and 82FR-31NR cells. Radiation activates the p53 pathway to induce apoptosis in irradiated parental cells. On the other hand, the AKT/cyclin D1/Cdk4 pathway is activated by irradiation in 82FR-31NR cells. The AKT pathway facilitates DNA repair of radiation-induced DNA damage and promotes cell survival in 82FR-31NR cells after irradiation.

pathway with API-2 or cyclin D1 siRNA. Thus, targeting the AKT pathway has the potential to induce cell death in CSCs by inhibiting efficient DNA repair, which is essential for protection of cells from irradiation.

AKT, cyclin D1and Cdk4 are molecular targets for eradication of CSC by RT

It is important to identify specific components of signal transduction pathway that is involved in radioresistance of CSCs. It was reported that the inhibition of the AKT pathway prevents neurosphere formation of glioblastoma cells and decreases cell growth of CD133-positive cells compared with CD133-negative cells.[29] Inhibition of the PI3K/AKT pathway sensitizes CSCs to both radiation and anti-cancer drugs with induction of apoptosis *in vivo*.[30,31] The PI3K/AKT pathway promotes chemo-resistance by regulating the ABC transporter BCRP1 activity, which enhances drug efflux.[32–34] In the present study, we have further demonstrated that cyclin D1/Cdk4 is the most important target downstream AKT to suppress radioresistance of CSCs. Thus, manipulation of cyclin D1 and Cdk4 may be useful to enhance radio- and chemo-sensitivity in CSCs. A number of therapeutic agents have been shown to induce cyclin D1 degradation.[35] Cdk4 inhibitor is also considerable for treatment of mantle cell lymphoma and is now under phase 1 study.[36,37] In the future study, careful evaluation is required to confirm the efficacy of these cyclinD1/Cdk4-targeting drugs combined with fractionated RT.

We have reported that the constitutively activated AKT/cyclin D1 pathway is associated with acquired radioresistance of tumor cells induced by exposure to FR for 31 days.[16] Because of CD133-negative in 31FR cells, cells with acquired radioresistance are different from CSCs. Furthermore, cells with acquired radioresistance harbor constitutive activation of the AKT/cyclin D1 pathway mediated by the cyclin D1 overexpression cycle, whereas AKT activation and cyclin D1 overexpression were not observed in non-irradiated 82FR-31NR cells as well as in non-irradiated parental cells. Our present data demonstrated that the AKT pathway is important not only in acquisition of radioresistance but also in radioresistance of CSCs. Thus, the AKT, cyclin D1 and Cdk4 are commonly implicated in intrinsic radioresistance of CSCs and acquired radioresistance by FR. Therefore, those molecules are attractive as therapeutic targets to overcome tumor radioresistance.

In conclusion, we have demonstrated that the AKT/cyclin D1/Cdk4 pathway may serve as a new target to enhance efficacy of RT by suppressing radioresistance of CSCs.

MATERIALS AND METHODS

Cell culture condition and drugs

HepG2, a human liver cancer cell line was obtained from the Cell Resource Center for Biomedical Research, IDAC, Tohoku University. A human glioblastoma cell line A172 was purchased from Japan Collection of Research Biosciences (Tokyo, Japan). Cells were grown in a RPMI1640 medium (NacalaiTesque, Kyoto, Japan) supplemented with 5% heat-inactivated fetal calf serum. An AKT inhibitor, API-2, and a Cdk4 inhibitor, Cdk4-I, were purchased from Calbiochem (San Diego, CA, USA). Rapamycin was purchased from Sigma (St Louis, MO, USA).

Irradiation experiments

Irradiation was performed using a 150-KVp X-ray generator (Model MBR-1520R, Hitachi, Tokyo, Japan) with a 0.5 mm Cu and 0.1 mm Al filter at a dose rate of 1.0 Gy per min.

Western blot analyses

Western blotting was performed as described previously.[38] Proteins were separated by sodium-lauryl-sulfate-polyacrylamide gel electrophoresis and transferred electrophoretically to PVDF membranes (Bio-Rad, Richmond, CA, USA). Membranes were blocked with 5% (w/v) phospho-blocker (Cell Biolabs. Inc., San Diego, CA, USA) for 1 h and incubated with each primary antibody, such as anti-β-actin (A2066, Sigma), anti-phospho-AKT-Ser473 (4060, Cell Signaling, Beverly, MA, USA), anti-AKT (4685, Cell Signaling), anti-CD133 (3663, Cell Signaling), anti-cyclin D1 (Nichirei Bioscience, Tokyo, Japan), anti-γ-H2AX (Upstate, Lake Placid, NY, USA), anti-p53 (DAKO, Glostrup, Denmark), anti-phospho-S6-Ser240/244 (2215, Cell Signaling), anti-S6 (2211, Cell Signaling), anti-phospho-P70S6K-Thr389 (9205, Cell Signaling) and anti-P70S6K (9209, Cell Signaling) for 1 h at room temperature or overnight at 4 °C. Membranes were then incubated for 1 h at room temperature with the secondary antibody of HRP-conjugated goat anti-rabbit IgG (Nichirei Bioscience) or HRP-conjugated goat anti-mouse IgG (R&D Systems, Minneapolis, MN, USA). The protein bands were visualized with Chemi-Lumi One L western blotting substrate (NacalaiTesque). Band intensity was measured by densitometry using Multi Gauge Analyses software (Fuji Film, Tokyo, Japan).

Flow cytometry analysis of CD133 expression

Cells were stained with phycoerythrin-conjugated anti-CD133 antibody (MilyenyiBiotec Inc., Auburn, CA, USA) following the manufacturer's protocol. Samples were analyzed on the FACScan (Cytomics FC500, Becton Dickinson, Mountain View, CA, USA).

Reverse transcription PCR

The expression of each gene was examined by RT (reverse transcription)–PCR. The primer sets used in the present analysis were as follows. Albumin: 5′-CGGCTTATTCCAGGGGTGTG-3′ and 5′-GGGGGAGGTTTGGGTTGTC-3′; BCRP1: 5′-AGATGGGTTTCCAAGCGTTCAT-3′ and 5′-CCAGTCCCAGTACGAC TGTGACA -3′; CD133: 5′-CATAAAGCTGGACCCATTGG-3′ and 5′-CCTTGTCC TTGGTAGTGTTG-3′; GADPH: 5′-GCCAAAAGGGTCATCATCTC-3′ and 5′-GTA GAGGCAGGGATGATGTTC -3′; GFAP: 5′-GCTCGATCAACTCACCGCCAACA-3′ and 5′-GGGCAGCAGCGTCTGTCAGGTC-3′; MDR1: 5′-ATATCAGCAGCCCAC ATCAT-3′ and 5′-GAAGCACTGGGATGTCCGGT -3′;

The PCR products were separated by electrophoresis in 1% agarose gel.

Immunofluorescence staining

Immunofluorescence staining was performed as described previously.[39] Cells were grown on 18 mm × 18 mm cover slips. Cells were fixed in 4% (w/v) paraformaldehyde in phosphate buffered saline (PBS) for 10 min, washed in PBS, made permeable in 0.25% Triton X-100 for 10 min, and then washed and blocked with PBS containing 5% bovine serum albumin for 15 min (permeabilization was omitted for CD133 staining). Cells were incubated with anti-CD133 (130-090-851, MilyenyiBiotec Inc.) or anti-cytokeratin14 (MAB3232, Millipore) antibodies. Antibodies were diluted in PBS with 0.5% bovine serum albumin for 1 h at 37 °C. Slides were then washed three times with 0.1% Triton X-100 in PBS and incubated for 1 h at

37 °C with secondary antibody conjugated with Alexa 488 (Molecular Probes, Eugene, OR, USA) or Cy-3 (Jackson Immuno Research Laboratories, Westgrove, PA, USA). Slides were washed three times with 0.1% Triton X-100 in PBS and counterstained for DNA with Hochest33258 (Wako Pure Chemical Industries, Ltd., Osaka, Japan). Images were captured by an epifluorescense microscopy (Nikon, Tokyo, Japan) using a $\times 40$ objective lens.

Clonogenic assay

Cells were seeded in 60-mm dish coated with 0.1% gelatin (Wako Pure Chemical Industries, Ltd) at 1×10^3 cells per dish. After irradiation, cells were incubated for 10 days until colonies were visible. They were fixed with ethanol for 30 min and stained with Giemsa solution (Merck & Co. Inc. Pennsylvania, PA, USA). The colonies of >50 cells were counted under a light microscope.

Annexin V staining

Apoptotic cells were identified and quantified using an annexin V-FITC apoptosis detection kit (Bio Vision, Mountain View, CA, USA) following the manufacturer's protocol. Cells were stained with annexin V-FITC and propidium iodide 48 h after treatment with radiation. Annexin V positive apoptotic cells were analyzed by the FACScan (Becton Dickinson).

RNA interference

Cells were transfected with siRNA using a Lipofectamine RNAiMAX reagent (Invitrogen, Carlsbad, CA, USA). Cyclin D1 siRNA, Cdk4 siRNA and control siRNA were purchased from Santa Cruz Biotechnology (Santa Cruz, CA, USA).

Animal experiments

The study design was approved by the Ethical Committee of IDAC, Tohoku University. Male BALB/c nu/nu mice of 5 weeks of age were used in the present experiment. All mice were maintained in our animal facility on a 12 light and 12 dark hour cycle under a controlled temperature (23 ± 2 °C). For the transplantation, 5×10^5 cells of 0FR and 82FR-31NR of HepG2 and A172 in 100 μl of saline were injected into the right and the left legs of the mice, respectively.

Cell growth assay

Cells (5×10^5) were seeded in a 25 cm^2 flask (Thermo Fisher Scientific/Nunc, Waltham, MA, USA), incubated overnight and irradiated daily with 2 Gy of FR for the indicated number of days. Growth rates were monitored by counting cell number twice a week. When the total cell number was over 5×10^5, cells were sub-cultured to 5×10^5 cells in a flask.

Statistical analysis

Error bars represent standard deviations; in some cases the standard deviations were too small to be visible on the histogram. All the experiments were repeated at least three times with independent samples. Student's *t*-test was used for the analysis. A single asterisk and double asterisks indicate the significance, ($P<0.01$) and ($P<0.05$), respectively.

CONFLICT OF INTEREST

The authors declare no conflict of interest.

ACKNOWLEDGEMENTS

This study was partly supported by the Grant-in-Aid from the Ministry of Education, Culture, Sports, Science and Technology, for Cancer Research from the Ministry of Health, Labour and Welfare, Research Seeds Quest Program of JST, Radiation Effect Association and Mishima Kaiun Memorial Foundation of Japan.

REFERENCES

1 Kim JJ, Tannock IF. Repopulation of cancer cells during therapy: an important cause of treatment failure. *Nat Rev Cancer* 2005; **5**: 516–525.
2 Pardal R, Clarke MF, Morrison SJ. Applying the principles of stem-cell biology to cancer. *Nat Rev Cancer* 2003; **3**: 895–902.
3 Nguyen GH, Murph MM, Chang JY. Cancer stem cell radioresistance and enrichment: where frontline radiation therapy may fail in lung and esophageal cancers. *Cancers* 2011; **3**: 1232–1252.
4 Bao SD, Wu QL, McLendon RE, Hao YL, Shi Q, Hjelmeland AB *et al.* Glioma stem cells promote radioresistance by preferential activation of the DNA damage response. *Nature* 2006; **444**: 756–760.
5 Baumann M, Krause M, Hill R. Exploring the role of cancer stem cells in radioresistance. *Nat Rev Cancer* 2008; **8**: 545–554.
6 Phillips TM, McBride WH, Pajonk F. The response of CD24(−/low)/CD44(+) breast cancer-initiating cells to radiation. *JNatl Cancer Inst* 2006; **98**: 1777–1785.
7 Tu LC, Foltz G, Lin E, Hood L, Tian Q. Targeting stem cells-clinical implications for cancer therapy. *Curr Stem Cell Res Ther* 2009; **4**: 147–153.
8 Dubrovska A, Kim S, Salamone RJ, Walker JR, Maira SM, Garcia-Echeverria C *et al.* The role of PTEN/Akt/PI3K signaling in the maintenance and viability of prostate cancer stem-like cell populations. *Proc Natl Acad Sci USA* 2009; **106**: 268–273.
9 Korkaya H, Paulson A, Charafe-Jauffret E, Ginestier C, Brown M, Dutcher J *et al.* Regulation of mammary stem/progenitor cells by PTEN/Akt/beta-Catenin signaling. *Plos Biology* 2009; **7**: e1000121.
10 Xu Q, Simpson SE, Scialla TJ, Bagg A, Carroll M. Survival of acute myeloid leukemia cells requires PI3 kinase activation. *Blood* 2003; **102**: 972–980.
11 Schmidt-Ullrich RK, Contessa JN, Dent P, Mikkelsen RB, Valerie K, Reardon DB *et al.* Molecular mechanisms of radiation-induced accelerated repopulation. *Radiat Oncol Investig* 1999; **7**: 321–330.
12 Dent P, Yacoub A, Contessa J, Caron R, Amorino G, Valerie K *et al.* Stress and radiation-induced activation of multiple intracellular signaling pathways. *Radiat Res* 2003; **159**: 283–300.
13 Manning BD, Cantley LC. AKT/PKB signaling: navigating downstream. *Cell* 2007; **129**: 1261–1274.
14 Vivanco I, Sawyers CL. The phosphatidylinositol 3-kinase-AKT pathway in human cancer. *Nat Rev Cancer* 2002; **2**: 489–501.
15 Musgrove EA, Caldon CE, Barraclough J, Stone A, Sutherland RL. Cyclin D as a therapeutic target in cancer. *Nat Rev Cancer* 2011; **11**: 558–572.
16 Shimura T, Kakuda S, Ochiai Y, Nakagawa H, Kuwahara Y, Takai Y *et al.* Acquired radioresistance of human tumor cells by DNA-PK/AKT/GSK3 beta-mediated cyclin D1 overexpression. *Oncogene* 2010; **29**: 4826–4837.
17 Shimura T, Kakuda S, Ochiai Y, Kuwahara Y, Takai Y, Fukumoto M. Targeting the AKT/GSK3 beta/cyclin D1/Cdk4 survival signaling pathway for eradication of tumor radioresistance acquired by fractionated radiotherapy. *Int J Radiat Oncol Biol Phys* 2011; **80**: 540–548.
18 Wu YJ, Wu PY. CD133 as a marker for cancer stem cells: progresses and concerns. *Stem Cells Dev* 2009; **18**: 1127–1134.
19 Pilch DR, Sedelnikova OA, Redon C, Celeste A, Nussenzweig A, Bonner WM. Characteristics of gamma-H2AX foci at DNA double strand breaks sites. *Biochem Cell Biol* 2003; **81**: 123–129.
20 Sedelnikova OA, Pilch DR, Redon C, Bonner WM. Histone H2AX in DNA damage and repair. *Cancer Biol Ther* 2003; **2**: 233–235.
21 Ma L, Lai DM, Liu T, Cheng WW, Guo LH. Cancer stem-like cells can be isolated with drug selection in human ovarian cancer cell line SKOV3. *Acta Biochim Biophys Sin* 2010; **42**: 593–602.
22 Mihatsch J, Toulany M, Bareiss PM, Grimm S, Lengerke C, Kehlbach R *et al.* Selection of radioresistant tumor cells and presence of ALDH1 activity *in vitro*. *Radiother Onco* 2011; **99**: 300–306.
23 Che SM, Liu XL, Chen X, Hou L, Zhang XZ. The radiosensitization effect of NS398 on esophageal cancer stem cell-like radioresistant cells. *Dis Esophagus* 2011; **24**: 265–273.
24 Hermann PC, Huber SL, Herrler T, Aicher A, Ellwart JW, Guba M *et al.* Distinct populations of cancer stem cells determine tumor growth and metastatic activity in human pancreatic cancer. *Cell Stem Cell* 2007; **1**: 313–323.
25 Wollman R, Yahalom J, Maxy R, Pinto J, Fuks Z. Effect of epidermal growth-factor on the growth and radiation sensitivity of human breast-cancer cells *in-vitro*. *Int J Radiat Oncol Biol Phys* 1994; **30**: 91–98.
26 Paris F, Fuks Z, Kang A, Capodieci P, Juan G, Ehleiter D *et al.* Endothelial apoptosis as the primary lesion initiating intestinal radiation damage in mice. *Science* 2001; **293**: 293–297.
27 Kao GD, Jiang Z, Fernandes AM, Gupta AK, Maity A. Inhibition of phosphatidylinositol-3-OH kinase/Akt signaling impairs DNA repair in glioblastoma cells following ionizing radiation. *J Biol Chem* 2007; **282**: 21206–21212.
28 Jirawatnotai S, Hu YD, Michowski W, Elias JE, Becks L, Bienvenu F *et al.* A function for cyclin D1 in DNA repair uncovered by protein interactome analyses in human cancers. *Nature* 2011; **474**: 230–234.
29 Eyler CE, Foo WC, Lafiura KM, McLendon RE, Hjelmeland AB, Rich JN. Brain cancer stem cells display preferential sensitivity to Akt inhibition. *Stem Cells* 2008; **26**: 3027–3036.

30 Hambardzumyan D, Becher OJ, Rosenblum MK, Pandolfi PP, Manova-Todorova K, Holland EC. PI3K pathway regulates survival of cancer stem cells residing in the perivascular niche following radiation in medulloblastoma *in vivo*. *Genes Dev* 2008; **22**: 436–448.
31 Ma S, Lee TK, Zheng BJ, Chan K, Guan XY. CD133(+) HCC cancer stem cells confer chemoresistance by preferential expression of the Akt/PKB survival pathway. *Oncogene* 2008; **27**: 1749–1758.
32 Bleau AM, Hambardzumyan D, Ozawa T, Fomchenko EI, Huse JT, Brennan CW *et al.* PTEN/PI3K/Akt pathway regulates the side population phenotype and ABCG2 activity in glioma tumor stem-like cells. *Cell Stem Cell* 2009; **4**: 226–235.
33 Mogi M, Yang J, Lambert JF, Colvin GA, Shiojima I, Skurk C *et al.* Akt signaling regulates side population cell phenotype via Bcrp1 translocation. *J Biol Chem* 2003; **278**: 39068–39075.
34 Takada T, Suzuki H, Gotoh Y, Sugiyama Y. Regulation of the cell surface expression of human BCRP/ABCG2 by the phosphorylation state of Akt in polarized cells. *Drug Metab Dispos* 2005; **33**: 905–909.
35 Alao JP. The regulation of cyclin D1 degradation: roles in cancer development and the potential for therapeutic invention. *Mol Cancer* 2007; **6**: 24.
36 Korz C, Pscherer A, Benner A, Mertens D, Schaffner C, Leupolt E *et al.* Evidence for distinct pathomechanisms in B-cell chronic lymphocytic leukemia and mantle cell lymphoma by quantitative expression analysis of cell cycle and apoptosis-associated genes. *Blood* 2002; **99**: 4554–4561.
37 Marzec M, Kasprzycka M, Lai R, Gladden AB, Wlodarski P, Tomczak E *et al.* Mantle cell lymphoma cells express predominantly cyclin D1a isoform and are highly sensitive to selective inhibition of CDK4 kinase activity. *Blood* 2006; **108**: 1744–1750.
38 Shimura T, Toyoshima M, Adiga SK, Kunoh T, Nagai H, Shimizu N *et al.* Suppression of replication fork progression in low-dose-specic p53-dependent S-phase DNA damage checkpoint. *Oncogene* 2006; **25**: 5921–5932.
39 Shimura T, Torres MJ, Martin MM, Rao VA, Pommier Y, Katsura M *et al.* Bloom's syndrome helicase and Mus81 are required to induce transient double-strand DNA breaks in response to DNA replication stress. *J Mol Biol* 2008; **375**: 1152–1164.

Cold-inducible RNA-binding protein (Cirp) interacts with Dyrk1b/Mirk and promotes proliferation of immature male germ cells in mice

Tomoko Masuda[a], Katsuhiko Itoh[a,1], Hiroaki Higashitsuji[a], Hisako Higashitsuji[a], Noa Nakazawa[a], Toshiharu Sakurai[a], Yu Liu[a], Hiromu Tokuchi[a], Takanori Fujita[a], Yan Zhao[a], Hiroyuki Nishiyama[b], Takashi Tanaka[c], Manabu Fukumoto[d], Masahito Ikawa[e], Masaru Okabe[e], and Jun Fujita[a,1]

[a]Department of Clinical Molecular Biology, Graduate School of Medicine, Kyoto University, Kyoto 606-8507, Japan; [b]Department of Urology, Graduate School of Comprehensive Human Sciences, University of Tsukuba, Tsukuba 3058575, Japan; [c]Department of Molecular Genetics, Graduate School of Medicine, Kyoto University, Kyoto 606-8507, Japan; [d]Department of Pathology, Institute of Development, Aging, and Cancer, Tohoku University, Sendai 980-8575, Japan; and [e]Department of Experimental Genome Research, Genome Information Research Center, Osaka University, Osaka 565-0871, Japan

Edited by Ralph L. Brinster, University of Pennsylvania, Philadelphia, PA, and approved May 24, 2012 (received for review December 30, 2011)

Cold-inducible RNA-binding protein (Cirp) was the first cold-shock protein identified in mammals. It is structurally quite different from bacterial cold-shock proteins and is induced in response to mild, but not severe, hypothermia. To clarify the physiological function of Cirp in vivo, we produced *cirp*-knockout mice. They showed neither gross abnormality nor defect in fertility, but the number of undifferentiated spermatogonia was significantly reduced and the recovery of spermatogenesis was delayed after treatment with a cytotoxic agent, busulfan. Cirp accelerated cell-cycle progression from G0 to G1 as well as from G1 to S phase in cultured mouse embryonic fibroblasts. Cirp directly bound to dual-specificity tyrosine-phosphorylation–regulated kinase 1B (Dyrk1b, also called Mirk) and inhibited its binding to p27, resulting in decreased phosphorylation and destabilization of p27. Cirp did not affect binding of Dyrk1b to cyclin D1 but inhibited phosphorylation of cyclin D1 by Dyrk1b, resulting in cyclin D1 stabilization. In the spermatogonial cell line GC-1spg, suppression of Cirp expression increased the protein level of p27, decreased that of cyclin D1, and decreased the growth rate, which depended on Dyrk1b. Consistent changes in the protein levels of p27 and cyclin D1 as well as the percentage of cells in G0 phase were observed in undifferentiated spermatogonia of *cirp*-knockout mice. In undifferentiated spermatogonia of wild-type mice, Cirp and Dyrk1b colocalized in the nucleus. Thus, our study demonstrates that Cirp functions to fine-tune the proliferation of undifferentiated spermatogonia by interacting with Dyrk1b.

In most mammals, the testes are located in the scrotum, wherein the temperature is below that of the body cavity by 2 °C to 7 °C (1). Scrotal testes become aspermatogenic if their temperature is raised to body temperature or above, either by artificial heat or by retaining them in the abdomen (2, 3). We previously identified the first mammalian cold-shock protein in the testis and named it cold-inducible RNA-binding protein (Cirp, also called Cirbp or hnRNP A18) (4). It is constitutively expressed in the male germ cells and inducibly expressed in almost all cell types by lowering the culture temperature to 32 °C but not below 20 °C. Expression of Cirp is also induced by cellular stresses such as UV irradiation and hypoxia (5–7). In response to the stress, Cirp migrates from the nucleus to cytoplasm and affects expression of its target mRNAs (8, 9). Cirp affects cell growth and protects cells from damages induced by tumor necrosis factor α, genotoxic stress, or cryptorchidism (4, 10–13).

In an adult mouse testis, spermatogenesis is sustained by germ-line stem cells (A_{single}) that undergo mitosis and self-renew or differentiate into committed A_{paired} and $A_{aligned}$ spermatogonia, which are collectively called undifferentiated spermatogonia (14). Undifferentiated spermatogonia constitute the smallest population, less than 1%, of total testicular cells, include cells with stem-cell function, and differentiate into differentiating spermatogonia (A_{1-4}, intermediate, and B), which will undergo meiosis after the final mitosis (15, 16). Recently, methods to enrich undifferentiated spermatogonia by flow cytometry using combinations of markers such as c-Kit and α6-integrin and the side population phenotype have been developed (17, 18).

Dual-specificity tyrosine-phosphorylation–regulated kinase 1B (Dyrk1b, also called Mirk) is a member of the conserved Dyrk/minibrain family of tyrosine-regulated, arginine-directed serine/threonine protein kinases (19). The highest level of Dyrk1b mRNA is observed in the testis and skeletal muscle, and Dyrk1b protein mediates muscle differentiation, cell survival, and cell migration (19). Biochemical analysis has revealed that Dyrk1b phosphorylates and blocks degradation of the cyclin-dependent kinase (CDK) inhibitor p27 in nontransformed cells that helps to maintain a quiescent state (20). Dyrk1b blocks quiescent cells from traversing G1 phase of the cell cycle by phosphorylating and destabilizing cyclin D1 and cyclin D3 (21).

In the present study, we have generated Cirp-deficient mice to clarify the biological function of mammalian cold-shock protein in vivo. We found that Cirp interacts with Dyrk1b and that it is required to fully maintain the undifferentiated spermatogonia.

Results

Number of Undifferentiated Spermatogonia Is Decreased in Cirp-Deficient Mice. We generated Cirp-deficient mice by homologous recombination in ES cells (Fig. 1*A*). Intercrossing of heterozygous mutant mice generated progeny at nearly Mendelian ratios ($cirp^{+/+}$:$cirp^{+/-}$:$cirp^{-/-}$ = 58:110:47, n = 215), and $cirp^{-/-}$ mice were indistinguishable from wild-type littermates in appearance. When we examined fertility of $cirp^{-/-}$ male mice by mating them with wild-type females, the litter size (average = 5.1 mice, n = 18) was not different from that of wild-type mating (average = 4.9 mice, n = 15). We observed no reproductive defect in $cirp^{-/-}$ females, either. Although the testis of $cirp^{-/-}$ mice looked histologically normal and the numbers of total testicular cells and differentiating spermatogonia as well as the size and weight of the testis were comparable to wild type, the percentage and number of c-Kit$^-$ and highly α6-integrin$^+$ undifferentiated spermatogonia in the

Author contributions: K.I. and J.F. designed research; T.M., K.I., Hiroaki Higashitsuji, Hisako Higashitsuji, N.N., T.S., Y.L., H.T., T.F., Y.Z., T.T., M.F., M.I., and M.O. performed research; T.M., K.I., H.N., and J.F. analyzed data; and T.M., K.I., M.O., and J.F. wrote the paper.

The authors declare no conflict of interest.

This article is a PNAS Direct Submission.

[1]To whom correspondence may be addressed. E-mail: jfujita@virus.kyoto-u.ac.jp or katsu@virus.kyoto-u.ac.jp.

This article contains supporting information online at www.pnas.org/lookup/suppl/doi:10.1073/pnas.1121524109/-/DCSupplemental.

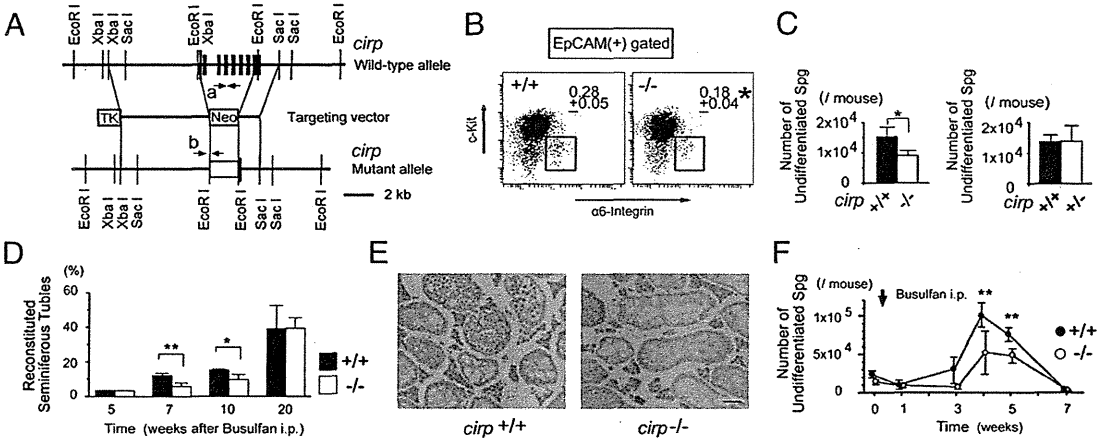

Fig. 1. Reduced number of undifferentiated spermatogonia in *cirp*-knockout mice. (*A*) Targeted disruption of the *cirp* gene. Structures of the wild-type allele, targeting vector, and mutant allele are shown together with the relevant restriction sites. The filled rectangles indicate the exons of the *cirp* gene. Neo, TK, and arrows (a and b) indicate a pgk-neo selection cassette, a thymidine kinase cassette, and the locations of primers for genomic PCR, respectively. (*B*) Flow cytometric analysis of undifferentiated spermatogonia. The fractions of undifferentiated spermatogonia (boxed) were compared between wild-type (+/+) and *cirp*-knockout (–/–) mice. *Significantly different from +/+ mice ($P < 0.05$). Data are from four +/+ and three –/– 12-wk-old mice. (*C*) Numbers of undifferentiated spermatogonia in +/+, –/–, and heterozygous knockout (+/–) mice. Significant decrease (*$P < 0.05$) was seen in –/– mice but not in +/– mice ($P = 0.93$). Values represent mean ± SD. Data are from eight +/+, three –/–, and four +/– mice. (*D*) Percentage of reconstituted seminiferous tubules after busulfan treatment. *Significantly different ($P < 0.05$). **Significantly different ($P < 0.01$). Values are mean ± SD ($n = 3$ each). (*E*) Histological sections of the testes at 7 wk after busulfan treatment. Sections are stained with hematoxylin and eosin. (Scale bar: 50 μm.) (*F*) Numbers of undifferentiated spermatogonia after busulfan treatment. ● and ○ indicate the numbers in +/+ and –/– mice, respectively. Values represent mean ± SD ($n = 3$–7). **Significantly different between +/+ and –/– mice ($P < 0.01$).

testicular epithelial cell adhesion molecule (EpCAM)$^+$ cells (18, 22) were decreased in *cirp*$^{-/-}$ mice compared with those in wild-type mice ($P < 0.05$) (Fig. 1 *B* and *C*). The number of undifferentiated spermatogonia in *cirp*$^{+/-}$ mice, however, was not different from that in wild-type mice ($P = 0.925$).

To determine whether the observed decrease in the number of undifferentiated spermatogonia has biological meaning, we analyzed the recovery process of spermatogenesis after i.p. injection of the alkylating agent busulfan (30 mg/kg body weight). The percentage of seminiferous tubules showing spermatogenesis was less than 3% and not different between wild-type and *cirp*$^{-/-}$ mice at 5 wk after the injection (Fig. 1*D*). At 7 and 10 wk, however, significantly fewer tubules were reconstituted in *cirp*$^{-/-}$ mice compared with wild-type mice (Fig. 1*E*). Consistently, the number of undifferentiated spermatogonia was significantly less in *cirp*$^{-/-}$ mice at 4 and 5 wk after the busulfan treatment (Fig. 1*F*).

To assess whether stem cells of other cell lineages are affected by deficiency of Cirp, we analyzed purified bone marrow cells enriched with hematopoietic stem cells (23, 24). Their numbers were comparable between *cirp*$^{-/-}$ and wild-type mice (Fig. S1 *A* and *B*). The competitive reconstitution assay did not reveal any significant difference between them even with an additional irradiation of recipient mice (Fig. S1 *C* and *D*). In contrast to spermatogonia, *cirp* mRNA expression was barely detectable in the analyzed hematopoietic cells (Fig. S1*E*).

Cirp Accelerates Cell-Cycle Progression in Cultured Mouse Embryonic Fibroblasts (MEFs). To analyze the effect of Cirp in vitro, we made several MEF cell lines that inducibly change the protein level of Cirp (Fig. S2 *A* and *B*). As shown in Fig. 2*A*, *cirp*$^{-/-}$ MEFs proliferated faster when Cirp was expressed both at 32 °C and 37 °C. When expression of Cirp was suppressed by shRNAs at 32 °C, proliferation of *cirp*$^{+/+}$ MEFs was suppressed (Fig. 2*B*). The suppressive effect was reversed by expression of shRNA-insensitive Cirp construct (Fig. S2 *C* and *D*), suggesting that the observed effect was not attributable to off-target effects of shRNAs.

We next analyzed the effect of Cirp on the cell cycle by BrdU incorporation and propidium iodide staining. When exogenous Cirp was expressed in *cirp*$^{-/-}$ MEFs at 32 °C, the percentage of cells in G0/G1 phase was reduced and that in S phase increased significantly (Fig. 2*C*). Conversely, when expression of Cirp was suppressed in *cirp*$^{+/+}$ MEFs at 32 °C, the percentage of cells in G0/G1 phase was increased and that in S phase reduced significantly (Fig. 2*C*). The changes in the Cirp protein levels did not affect the percentage of the sub-G1 population (Fig. S3*A*). These results indicate that expression of Cirp accelerates the G0/G1-to-S phase transition without affecting apoptosis.

The cells with 2N DNA content and that are not positively stained with anti-Ki67 antibody are considered to be in the G0 phase of the cell cycle (25). The G0 state is characterized by significantly decreased ribosomal RNA synthesis and lowered total cellular protein content. When Cirp was expressed in *cirp*$^{-/-}$ MEFs, the percentage of cells in the fraction of Ki67^{low} or Ki67$^-$ was significantly decreased, and the percentage of cells highly positive for pyronin Y staining, which stains polysomal RNA, was increased (Fig. 2*D*). Conversely, the percentage of G0 cells was significantly increased when Cirp expression was suppressed in *cirp*$^{+/+}$ MEFs at 32 °C (Fig. 2*E*). These results demonstrate that Cirp accelerates cell-cycle progression from G0 to G1 as well as from G1 to S phase in cultured MEFs.

Cirp Binds to Dyrk1b and Inhibits Its Kinase Activity. Yeast two-hybrid screening of a mouse testis cDNA library using Cirp as bait suggested that the C-terminal glycine-rich domain of Cirp binds to Dyrk1b (Fig. S4*A*).

When exogenously expressed as GFP-fusion proteins in HEK293T cells, full-length Cirp and its glycine-rich domain, but not its N-terminal RNA-binding domain, were coimmunoprecipitated with Dyrk1b as expected (Fig. S4 *B* and *C*). The region of Dyrk1b that interacted with Cirp was the kinase domain (Fig. S4*D*). Binding of endogenous Cirp and Dyrk1b was detected in MEFs of the *cirp*$^{+/+}$ genotype cultured at 32 °C (Fig. S4*E*). The recombinant Cirp protein bound to recombinant Dyrk1b protein in vitro, indicating a direct interaction

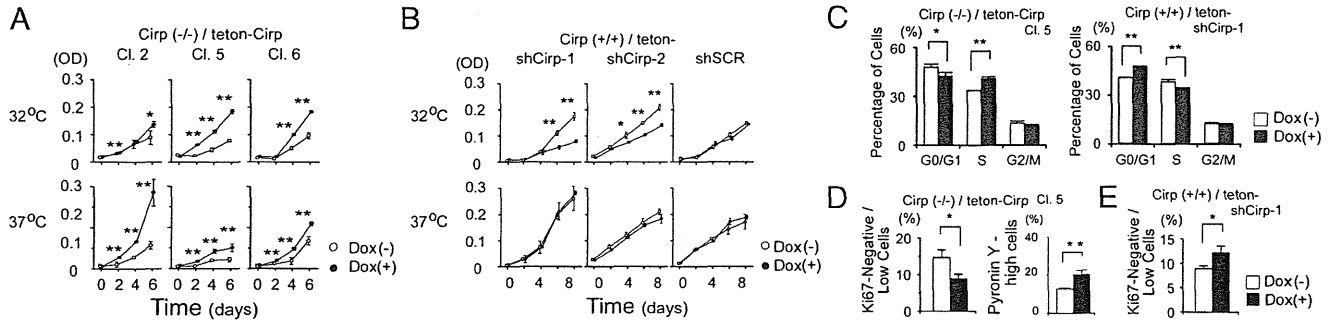

Fig. 2. Accelerated proliferation of MEFs expressing Cirp. (*A* and *B*) Effects of Cirp on cell growth. Cells from Cirp(–/–)/teton-Cirp clones 2, 5, and 6 (Cl. 2, Cl. 5, and Cl. 6, respectively) were derived from *cirp*$^{-/-}$ MEFs that express Cirp in the presence of Dox. Cirp(+/+)/teton-shCirp cells were derived from *cirp*$^{+/+}$ MEFs that Dox-inducibly express shRNAs that knockdown Cirp expression (shCirp-1 and shCirp-2) or scrambled RNAs (shSCR). Cells were cultured in the presence (+) or absence (–) of Dox at the indicated temperatures. Cell numbers were assessed by 3-(4,5-dimethylthiazol-2-yl)-2,5-diphenyltetrazolium bromide (MTT) assays. Values are mean ± SD (n = 3 or 4). *P < 0.05. **P < 0.01. (*C*) Analysis of the cell cycle by flow cytometry. BrdU incorporation and DNA content were analyzed in indicated cells cultured at 32 °C in the presence (+) or absence (–) of Dox. Percentages of cells in indicated phases of cell cycle are shown. Values are mean ± SD (n = 3). *P < 0.05. **P < 0.01. (*D* and *E*) Percentages of cells in G0 phase in the presence (+) or absence (–) of Dox. Ki67 expression, stainability with pyronin Y, and DNA content were analyzed in indicated cells by flow cytometry. Values are mean ± SD (n = 3). *P < 0.05.

(Fig. S4*F*). Immunocytochemistry demonstrated that Cirp was induced and colocalized with Dyrk1b in the nucleus at 32 °C in *cirp*$^{+/+}$ MEFs (Fig. S4*G*). In undifferentiated and differentiating spermatogonia, Cirp and Dyrk1b mRNAs were expressed, and their proteins were colocalized in the nucleus (Fig. S4 *H* and *I*).

Dyrk1b phosphorylates p27 and cyclin D1 to affect cell-cycle progression (19). When increasing amounts of Cirp were expressed in HEK293T cells, decreasing amounts of p27 were coimmunoprecipitated with Dyrk1b (Fig. 3*A*). In contrast, the amount of cyclin D1 coimmunoprecipitated with Dyrk1b was not decreased in the presence of Cirp and its binding to Dyrk1b (Fig. S5*A*). The presence of cyclin D1 did not affect the binding of Cirp to Dyrk1b either, and Cirp was coimmunoprecipitated with cyclin D1 as well (Fig. S5 *B* and *C*). These results indicate that Cirp forms a complex together with Dyrk1b and cyclin D1.

Dyrk1b immunoprecipitated from HEK293T cells could phosphorylate recombinant p27 in vitro (Fig. 3*B*). The amount of phosphorylated p27 was dose-dependently decreased in the presence of Cirp. When we incubated recombinant cyclin D1 with recombinant Dyrk1b, phosphorylation of cyclin D1 was observed (Fig. 3*C*). The phosphorylation was dose-dependently suppressed by Cirp. Interestingly, Cirp was also phosphorylated by Dyrk1b.

These data demonstrate that Cirp binds to and inhibits the kinase activity of Dyrk1b toward both p27 and cyclin D1, although Cirp competitively blocks the binding of Dyrk1b to p27 but not to cyclin D1.

Effects of Cirp on Cell-Cycle Progression Are Mediated by p27 and Cyclin D1 via Dyrk1b. Rapid removal of p27 at the G0/G1 transition and expression of cyclin D1 at the G1/S transition are required for effective progression of the cell cycle to S phase (26, 27). When Cirp was inducibly expressed with doxycycline (Dox) in *cirp*$^{-/-}$ MEFs, expression of p27 was decreased and that of cyclin D1 was increased (Fig. 4*A*) because of the increased and decreased degradation rates of p27 and cyclin D1, respectively (Fig. S4 *J* and *K*). Conversely, when expression of Cirp was suppressed in *cirp*$^{+/+}$ MEFs, expression of p27 was increased and that of cyclin D1 was decreased (Fig. 4*A*).

Because p27 and cyclin D1 are known to be phosphorylated by kinases besides Dyrk1b (26, 27), we examined whether the effects of Cirp on p27 and cyclin D1 depended on Dyrk1b. We stably expressed shRNAs targeted to Dyrk1b mRNAs or scrambled shRNAs in *cirp*$^{-/-}$ MEFs that inducibly express Cirp (Fig. S5*D*). Induction of Cirp decreased the protein level of p27

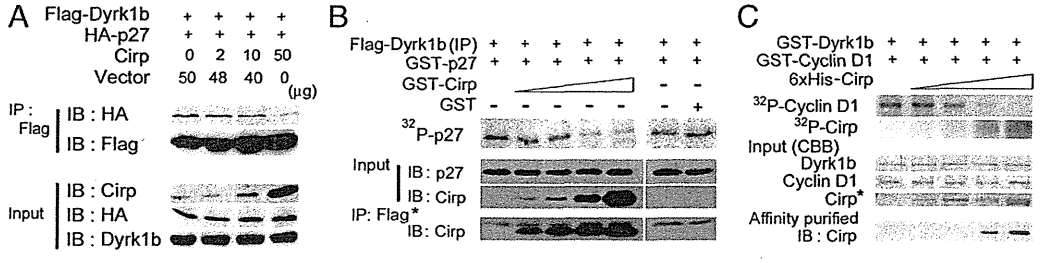

Fig. 3. Inhibition of Dyrk1b kinase activity by Cirp. (*A*) Effects of Cirp on binding of p27 to Dyrk1b. Plasmids were cotransfected into HEK293T cells as indicated. Proteins immunoprecipitated (IP) with anti-FLAG antibody and inputs were analyzed by Western blotting (IB) using the indicated antibodies. +, Present; –, absent. (*B*) Effects of Cirp on in vitro kinase activity of Dyrk1b toward p27. Immunoprecipitants (IP) were prepared from HEK293T cells expressing FLAG-Dyrk1b by using anti-FLAG antibody. Their kinase activity was assayed in the presence of [γ-^{32}P]ATP, GST-p27, and increasing amounts of GST-Cirp or GST. Reaction mixtures were separated by SDS/PAGE and analyzed by autoradiography. Proteins coprecipitated with protein G Sepharose beads (*) from the reaction mixtures without ^{32}P and inputs (2%) were analyzed by IB using the indicated antibodies. (*C*) Effects of Cirp on in vitro kinase activity of Dyrk1b toward cyclin D1. Recombinant GST-Dyrk1b was incubated with [γ-^{32}P]ATP, GST-cyclin D1, and increasing amounts of His-tagged Cirp and analyzed as in *B*. The lower images show Coomassie blue staining (CBB) of the indicated proteins used in the assay and IB of proteins coprecipitated with glutathione Sepharose beads from the reaction mixtures without ^{32}P (affinity-purified). *1/4 of input. Experiments were repeated three (*A*) and four (*B* and *C*) times, with similar results.

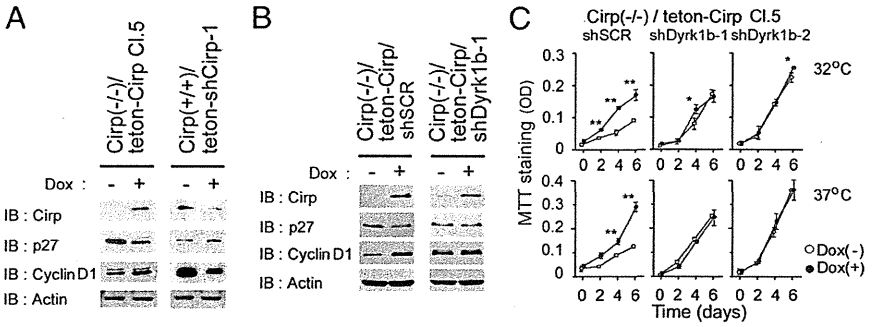

Fig. 4. Effects of Cirp on p27 and cyclin D1 via Dyrk1b in cultured MEFs. (*A*) Effects of Cirp on p27 and cyclin D1 protein levels. Cirp(–/–)/teton-Cirp Cl. 5 and Cirp(+/+)/teton-shCirp-1 cells were cultured at 32 °C in the presence (+) or absence (–) of Dox. Cell lysates were analyzed by IB using the indicated antibodies. (*B*) Dyrk1b dependency of protein levels. Indicated cells, both derived from Cirp(–/–)/teton-Cirp Cl. 5 cells, were cultured at 37 °C and analyzed as in *A*. (*C*) Dyrk1b and cell growth. Indicated cells were cultured at 32 °C and 37 °C in the presence (+) or absence (–) of Dox. Cell numbers were assessed by MTT assays. Values are mean ± SD ($n = 3$). $*P < 0.05$. $**P < 0.01$. Experiments were repeated four (*B*) and three (*C*) times, with similar results.

and increased that of cyclin D1 in *cirp*$^{-/-}$ MEFs expressing scrambled shRNAs (Fig. 4*B* and Fig. S5*E*). When expression of Dyrk1b was suppressed, however, Cirp did not show these effects in *cirp*$^{-/-}$ MEFs. The growth rate of these cells was not affected by Cirp either (Fig. 4*C*). These data demonstrate that expression of Cirp accelerates cell-cycle progression by inhibiting the kinase activity of Dyrk1b toward p27 and cyclin D1 in MEFs.

Down-Regulation of Cirp Suppresses Cell-Cycle Progression in a Spermatogonial Cell Line in Vitro and Undifferentiated Spermatogonia in Vivo. To analyze the effect of Cirp on male germ cells, we first used the mouse spermatogonial cell line GC-1spg (28). When GC-1spg cells were transduced with control retrovirus expressing scrambled shRNAs, expression of Cirp was induced at 32 °C like parental cells (Fig. S6*A*). In GC-1spg cells transduced with retrovirus expressing shRNAs to *cirp* mRNAs, the induction of Cirp was partly suppressed, the level of p27 protein was increased, and the level of cyclin D1 protein was decreased (Fig. S6*B*). These cells proliferated more slowly than the control cells (Fig. 5*A*). To confirm that growth-suppressive effect of Cirp down-regulation depends on Dyrk1b, we further down-regulated Dyrk1b expression (Fig. S6*C*). As shown in Fig. 5*B*, the impaired growth was rescued by suppressing the expression of Dyrk1b.

Next, we examined the effects of Cirp deficiency on the cell cycle in undifferentiated spermatogonia in vivo. At 4 wk after injection of busulfan, the percentage of Ki67^{+} cells was significantly smaller and the percentage of pyronin Y^{low} cells was significantly larger in undifferentiated spermatogonia isolated from *cirp*$^{-/-}$ mice than those from *cirp*$^{+/+}$ wild-type mice (Fig. 5*C*). RT-PCR analysis demonstrated that undifferentiated spermatogonia expressed mRNAs for p27 and cyclin D1 (Fig. 5*D*) as well as for Cirp and Dyrk1b. Furthermore, the protein level of p27 was higher and that of cyclin D1 was lower in undifferentiated spermatogonia of *cirp*$^{-/-}$ mice compared with those of wild-type mice, although the mRNA level for p27 was not different and that for cyclin D1 was higher in *cirp*$^{-/-}$ mice (Fig. 5*E* and Fig. S7 *A* and *B*). Altogether, these data indicate that Cirp destabilizes p27 and stabilizes cyclin D1 at the protein level in undifferentiated spermatogonia, resulting in an accelerated cell-cycle progression in wild-type mice and decreased proliferation in Cirp-deficient mice.

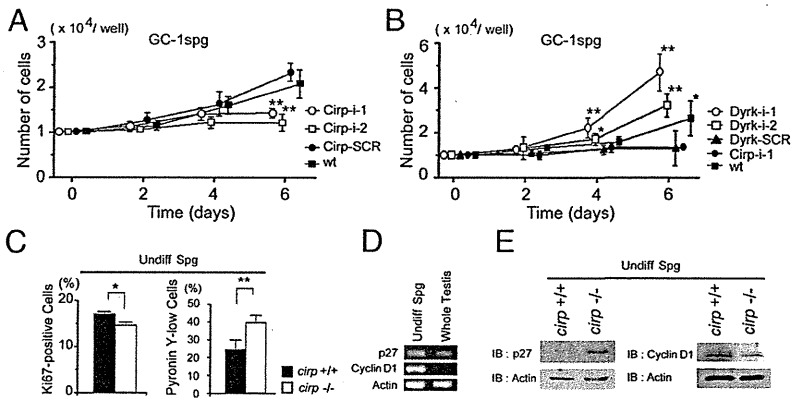

Fig. 5. Impaired cell-cycle progression in Cirp-deficient spermatogonia. (*A*) Effects of Cirp on growth of cultured GC-1spg cells. Cells were transduced with retrovirus [murine stem cell virus-LTRmiR30-PIG (MSCV-LMP)] expressing RNAi sequences targeted to Cirp (Cirp-i-1 and Cirp-i-2) or scrambled sequence (Cirp-SCR). Cells were cultured at 32 °C, and cell numbers were assessed by MTT assays. wt, untransduced cells. Values are mean ± SD ($n = 3$). $**P < 0.01$. (*B*) Dyrk1b-dependent effects of Cirp on growth of GC-1spg cells. Cirp-i-1 cells were further transduced with retrovirus [Friend spleen focus-forming virus-based hybrid vector 2 (SF2)] expressing RNAi sequences targeted to Dyrk1b (Dyrk-i-1 and Dyrk-i-2) or scrambled sequence (Dyrk-SCR) and analyzed as in *A*. (*C–E*) Undifferentiated spermatogonia of *cirp*$^{-/-}$ and *cirp*$^{+/+}$ genotypes were sorted and analyzed at 4 wk after busulfan treatment. (*C*) The percentages of Ki67^{+} (*Left*) and pyronin Y^{-} or pyronin Y^{low} (*Right*) cells were assessed by flow cytometry. Values are mean ± SD [$n = 3$ (*Left*) or 4 (*Right*)]. $*P < 0.05$ and $**P < 0.01$, respectively, different between wild-type (+/+) and *cirp*-knockout (–/–) mice. (*D*) Detection of p27 and cyclin D1 transcripts in spermatogonia isolated from *cirp*$^{-/-}$ mice. cDNAs were analyzed by RT-PCR. (*E*) Protein levels of p27 and cyclin D1. Cell lysates were analyzed by IB using the indicated antibodies. Experiments were repeated three times (*D* and *E*), with similar results.

Discussion

Numbers and Proliferative Activity of Undifferentiated Spermatogonia Are Decreased in *cirp*-Knockout Mice. In mammals, there have been only two established cold-shock proteins reported to date, Cirp and RNA-binding motif protein 3 (Rbm3), which are structurally quite similar (5). In the mouse testis, Cirp is constitutively expressed in the germ cells and the level varies depending on the stage of differentiation, whereas Rbm3 is suggested to be expressed mainly in the Sertoli cells (3, 29). When mouse testis is exposed to heat stress, expression of Cirp and Rbm3 is decreased, suggesting that the decreased expression might be related to the heat-induced testicular damage. Indeed, overexpression of Cirp has recently been reported to reduce the damage by cryptorchidism (13). In the present study, we found that the Cirp-deficient mice have reduced numbers of undifferentiated spermatogonia, although the total numbers of testicular germ cells and fertility were not significantly decreased. When they were exposed to the cytotoxic agent busulfan, the recovery of spermatogenesis was affected slightly but significantly. In addition to Cirp, Rbm3 was expressed in spermatogonia (Fig. S7 *C* and *D*). Because its expression level was not increased in spermatogonia of the $cirp^{-/-}$ genotype compared with those of wild type, it seems unlikely that the relatively mild defects observed in the knockout mice are a consequence of redundancy/compensation by Rbm3. Analysis of the *cirp* and *rbm3* double-knockout mice would clarify this possibility.

A vast majority of stem cell functions reside in the undifferentiated spermatogonia population (30). The findings that the undifferentiated spermatogonia expressed Cirp and that proliferation of the spermatogonial cell line was suppressed when Cirp expression was decreased suggest that the observed defect in $cirp^{-/-}$ mouse testis is mainly intrinsic to the spermatogonia rather than their environment. Consistent with this notion, no effect of Cirp deficiency was observed in hematopoietic stem cell populations that normally do not express Cirp.

Cells overexpressing Cirp are more resistant to various stresses, and down-regulation of Cirp inhibits cell growth in some cancer cells (31). We found that cell-cycle progression is inhibited at both G1-to-S and G0-to-G1 phase transitions with no change in the sub-G1 population in Cirp-deficient MEFs. Consistently, the proportion of undifferentiated spermatogonia in G0 phase was increased in $cirp^{-/-}$ mice compared with wild-type mice after treatment with busulfan. The numbers of apoptotic testicular cells were not apparently different between $cirp^{-/-}$ and wild-type mice after busulfan treatment, and the sensitivity of cultured MEFs of the $cirp^{-/-}$ genotype to busulfan was not affected by expression of Cirp (Fig. S3 *B* and *C*). In addition, expression of Cirp stimulated proliferation of the spermatogonial cell line. Thus, the decrease in the number of undifferentiated spermatogonia in $cirp^{-/-}$ mice could be considered mainly attributable to decreased cell proliferation rather than increased cell death.

The growth-stimulatory effects of Cirp on spermatogonia and MEFs seem contradictory to our original finding in BALB/3T3 cells (4) and consistent with the finding in CHO cells (32). We have also observed growth-suppressive effects of Cirp in NIH/3T3 and U-2 OS cells (Fig. S8*A*). Growth-stimulatory effects have been observed by others in PC3 and LNCaP human prostate cancer cells and MEFs, but not in NIH/3T3, HeLa, IMR90, or human mammary epithelial cells (10, 12). These two classes of cell lines that differently respond to Cirp expression were not distinguished by the protein levels of cyclin D1, CDK inhibitors such as p16 and p27, Dyrk1b, or Cirp (Fig. S8 *B* and *C*). Further studies are thus necessary to clarify this issue. Cirp probably fine-tunes the proliferation of cells by promoting and suppressing growth signals through distinct protein–protein and protein–RNA interactions, which depend on multiple factors, including the cell types, stresses, and conditions of cells.

Cirp Binds to and Inhibits the Kinase Activity of Dyrk1b Toward p27 and Cyclin D1. Dyrk1b autophosphorylates the second tyrosine in the Tyr-X-Tyr motif, an event that is essential for full kinase activity (33). Once phosphorylated, Dyrk1b functions as a serine/threonine kinase. Ran-binding protein M (RanBPM) directly binds to Dyrk1b and inhibits its kinase activity toward hepatocyte nuclear factor 1α (HNF1α) (34). In contrast, direct binding to dimerization cofactor of HNF1 from muscle (DCoHm) potentiates Dyrk1b's activity as an activator of HNF1α (35). Although phosphorylation of RanBPM or DCoHm by Dyrk1b has not been detected (34), we found that Cirp directly binds to and is phosphorylated by Dyrk1b, resulting in inhibition of its kinase activity toward p27 and cyclin D1.

p27 opposes cell-cycle progression by inhibiting cyclin E/Cdk2 (27). The expression level of p27 is high during G0 phase but decreases rapidly on reentry of the cells into G1 phase. Ser^{10} is the major site of p27 phosphorylation by Dyrk1b in resting cells that leads to protein stability (20). Previous studies have suggested a role of p27 in male germ-cell development. Mice deficient in S-phase kinase-associated protein 2 (Skp2), which mediates ubiquitin-dependent degradation of p27, exhibit a progressive loss in spermatogenic cells (36). Conversely, testes from p27-knockout mice are significantly larger (37) and contain increased numbers of type A spermatogonia (38), and $EpCAM^{+}$ spermatogonia from the knockout mice proliferate more actively than those from wild-type mice do (39). We found that Cirp decreases the protein level of p27 and increases cell proliferation via Dyrk1b in MEFs and the spermatogonial cell line and that the p27 protein level and cells in G0 phase were increased in Cirp-deficient undifferentiated spermatogonia. These results strongly suggest that the absence of Cirp increases phosphorylation of p27 by Dyrk1b, resulting in its stabilization and reduced cell-cycle progression in undifferentiated spermatogonia of the $cirp^{-/-}$ genotype.

D-type cyclins are G1-specific cyclins that associate with Cdk4 or Cdk6 and promote restriction point progression during G1 phase (40). In accordance with the immunohistochemical study by Beumer et al. (41), we detected expression of cyclin D1 in undifferentiated spermatogonia. The protein level of cyclin D1 was decreased in undifferentiated spermatogonia of $cirp^{-/-}$ mice compared with wild-type mice. Although binding to Cirp decreases the activity of Dyrk1b to phosphorylate cyclin D1 as well as to p27, the binding inhibits the binding of Dyrk1b to p27 but not to cyclin D1. After phosphorylation by Dyrk1b, p27 remains a functional CDK inhibitor, does not translocate from the nucleus, and colocalizes with Dyrk1b in G0 (20). Mitogen stimulation then causes cells to enter G1, reduces Dyrk1b levels (42), and initiates the translocation of p27 to the cytoplasm to be degraded. Thus, induction at moderately low temperatures, colocalization in the nucleus with Dyrk1b, and inhibition of Dyrk1b's binding to p27 would contribute to the ability of Cirp to enhance degradation of p27. Cyclin D1 is translocated into the cytoplasm during S phase, where it is destroyed by the proteasome after phosphorylation at Thr^{286} by glycogen synthase kinase 3. Dyrk1b phosphorylates cyclin D1 at Thr^{288}, which also enhances its rapid turnover (26). The nuclear complex formation of Dyrk1b, Cirp, and cyclin D1 would thus inhibit the nuclear export and degradation of cyclin D1. Although Cirp itself is a substrate and seems to compete with cyclin D1 for phosphorylation (Fig. 3*C*), it is also possible that Cirp has an independent mechanism for inhibiting Dyrk1b activity. The precise molecular mechanism by which Cirp inhibits the kinase activity of Dyrk1b remains to be elucidated.

In summary, we have demonstrated unique physiological function of the mammalian cold-shock protein Cirp that might

partly explain why testis should be kept cool. Cirp fine-tunes the cell-cycle progression of undifferentiated spermatogonia as well as fibroblasts and cancer cells by interacting with and suppressing kinase activity of Dyrk1b to modulate the protein levels of p27 and cyclin D1 (Fig. S9). Because Cirp affects proliferation of immature male germ cells and could act as an oncoprotein in some tumors, these findings may pave the way for development of new diagnoses and treatments for male infertility and cancers.

Materials and Methods

Generation of the Targeting Vector. The 6.4-kb XbaI/EcoRI fragment of the genomic DNA clones of the *cirp* locus (Fig. 1*A*) was inserted between the neomycin-resistance cassette and the HSV thymidine kinase gene, both of which are driven by the phosphoglycerate kinase 1 (PGK1) promoter, in the pPNT vector. The 1.4-kb EcoRI/SacI fragment was inserted upstream of the neomycin-resistance gene (Fig. 1*A*).

Isolation of Undifferentiated Spermatogonia. Isolation of undifferentiated spermatogonia was performed as described by Takubo et al. (18) with minor modifications.

Additional materials and experimental procedures are provided in *SI Materials and Methods*.

ACKNOWLEDGMENTS. We thank Dr. C. Toniatti and Dr. H. Bujard for the Bs/IRES-M2 plasmid; Dr. T. Shinohara, Dr. M. Sugai, and Dr. R. J. Mayer for helpful comments; and Dr. K. Nonoguchi for technical assistance. This work was supported in part by the Smoking Research Foundation of Japan, the Cooperative Research Project Program at the Institute of Development, Aging, and Cancer at Tohoku University; and Grants-in-Aid for Scientific Research (KAKENHI) from the Japan Society for the Promotion of Science.

1. Harrison RG, Weiner JS (1948) Abdomino-testicular temperature gradients. *J Physiol* 107:48–49.
2. Carrick F, Setchell B (1977) The evolution of the scrotum. *Reproduction and Evolution*, eds Calaby J, Tyndale-Biscoe T (Australian Academy of Science, Canberra), pp 165–170.
3. Nishiyama H, et al. (1998) Decreased expression of cold-inducible RNA-binding protein (CIRP) in male germ cells at elevated temperature. *Am J Pathol* 152:289–296.
4. Nishiyama H, et al. (1997) A glycine-rich RNA-binding protein mediating cold-inducible suppression of mammalian cell growth. *J Cell Biol* 137:899–908.
5. Fujita J (1999) Cold shock response in mammalian cells. *J Mol Microbiol Biotechnol* 1:243–255.
6. Wellmann S, et al. (2004) Oxygen-regulated expression of the RNA-binding proteins RBM3 and CIRP by a HIF-1-independent mechanism. *J Cell Sci* 117:1785–1794.
7. Yang C, Carrier F (2001) The UV-inducible RNA-binding protein A18 (A18 hnRNP) plays a protective role in the genotoxic stress response. *J Biol Chem* 276:47277–47284.
8. De Leeuw F, et al. (2007) The cold-inducible RNA-binding protein migrates from the nucleus to cytoplasmic stress granules by a methylation-dependent mechanism and acts as a translational repressor. *Exp Cell Res* 313:4130–4144.
9. Yang R, Weber DJ, Carrier F (2006) Post-transcriptional regulation of thioredoxin by the stress inducible heterogenous ribonucleoprotein A18. *Nucleic Acids Res* 34: 1224–1236.
10. Sakurai T, et al. (2006) Cirp protects against tumor necrosis factor-alpha-induced apoptosis via activation of extracellular signal-regulated kinase. *Biochim Biophys Acta* 1763:290–295.
11. Artero-Castro A, et al. (2009) Cold-inducible RNA-binding protein bypasses replicative senescence in primary cells through extracellular signal-regulated kinase 1 and 2 activation. *Mol Cell Biol* 29:1855–1868.
12. Zeng Y, Kulkarni P, Inoue T, Getzenberg RH (2009) Down-regulating cold shock protein genes impairs cancer cell survival and enhances chemosensitivity. *J Cell Biochem* 107:179–188.
13. Zhou KW, Zheng XM, Yang ZW, Zhang L, Chen HD (2009) Overexpression of CIRP may reduce testicular damage induced by cryptorchidism. *Clin Invest Med* 32:E103–E111.
14. Meistrich ML, van Beek MEAB (1993) Spermatogonial stem cells. *Cell and Molecular Biology of the Testis*, eds Desjardins C, Ewing LL (Oxford Univ Press, Oxford, UK), pp 266–294.
15. Nakagawa T, Nabeshima Y, Yoshida S (2007) Functional identification of the actual and potential stem cell compartments in mouse spermatogenesis. *Dev Cell* 12:195–206.
16. Oatley JM, Brinster RL (2006) Spermatogonial stem cells. *Methods Enzymol* 419:259–282.
17. Barroca V, et al. (2009) Mouse differentiating spermatogonia can generate germinal stem cells in vivo. *Nat Cell Biol* 11:190–196.
18. Takubo K, et al. (2008) Stem cell defects in ATM-deficient undifferentiated spermatogonia through DNA damage-induced cell-cycle arrest. *Cell Stem Cell* 2:170–182.
19. Friedman E (2007) Mirk/Dyrk1B in cancer. *J Cell Biochem* 102:274–279.
20. Deng X, Mercer SE, Shah S, Ewton DZ, Friedman E (2004) The cyclin-dependent kinase inhibitor p27(Kip1) is stabilized in G(0) by Mirk/dyrk1B kinase. *J Biol Chem* 279: 22498–22504.
21. Deng X, Ewton DZ, Friedman E (2009) Mirk/Dyrk1B maintains the viability of quiescent pancreatic cancer cells by reducing levels of reactive oxygen species. *Cancer Res* 69:3317–3324.
22. Anderson R, Schaible K, Heasman J, Wylie C (1999) Expression of the homophilic adhesion molecule, Ep-CAM, in the mammalian germ line. *J Reprod Fertil* 116: 379–384.
23. Osawa M, Hanada K, Hamada H, Nakauchi H (1996) Long-term lymphohematopoietic reconstitution by a single CD34-low/negative hematopoietic stem cell. *Science* 273:242–245.
24. Harrison DE (1980) Competitive repopulation: A new assay for long-term stem cell functional capacity. *Blood* 55:77–81.
25. Kubbutat MH, et al. (1994) Epitope analysis of antibodies recognising the cell proliferation associated nuclear antigen previously defined by the antibody Ki-67 (Ki-67 protein). *J Clin Pathol* 47:524–528.
26. Alao JP (2007) The regulation of cyclin D1 degradation: Roles in cancer development and the potential for therapeutic invention. *Mol Cancer* 6:24–39.
27. Larrea MD, Wander SA, Slingerland JM (2009) p27 as Jekyll and Hyde: Regulation of cell cycle and cell motility. *Cell Cycle* 8:3455–3461.
28. Hofmann MC, Narisawa S, Hess RA, Millán JL (1992) Immortalization of germ cells and somatic testicular cells using the SV40 large T antigen. *Exp Cell Res* 201:417–435.
29. Danno S, Itoh K, Matsuda T, Fujita J (2000) Decreased expression of mouse Rbm3, a cold-shock protein, in Sertoli cells of cryptorchid testis. *Am J Pathol* 156:1685–1692.
30. Nakagawa T, Sharma M, Nabeshima Y, Braun RE, Yoshida S (2010) Functional hierarchy and reversibility within the murine spermatogenic stem cell compartment. *Science* 328:62–67.
31. Lleonart ME (2010) A new generation of proto-oncogenes: Cold-inducible RNA binding proteins. *Biochim Biophys Acta* 1805:43–52.
32. Hong JK, Kim YG, Yoon SK, Lee GM (2007) Down-regulation of cold-inducible RNA-binding protein does not improve hypothermic growth of Chinese hamster ovary cells producing erythropoietin. *Metab Eng* 9:208–216.
33. Lochhead PA, Sibbet G, Morrice N, Cleghon V (2005) Activation-loop autophosphorylation is mediated by a novel transitional intermediate form of DYRKs. *Cell* 121: 925–936.
34. Zou Y, Lim S, Lee K, Deng X, Friedman E (2003) Serine/threonine kinase Mirk/Dyrk1B is an inhibitor of epithelial cell migration and is negatively regulated by the Met adaptor Ran-binding protein M. *J Biol Chem* 278:49573–49581.
35. Lim S, Jin K, Friedman E (2002) Mirk protein kinase is activated by MKK3 and functions as a transcriptional activator of HNF1alpha. *J Biol Chem* 277:25040–25046.
36. Fotovati A, Nakayama K, Nakayama KI (2006) Impaired germ cell development due to compromised cell cycle progression in Skp2-deficient mice. *Cell Div* 1:4–13.
37. Nakayama K, et al. (1996) Mice lacking p27(Kip1) display increased body size, multiple organ hyperplasia, retinal dysplasia, and pituitary tumors. *Cell* 85:707–720.
38. Beumer TL, et al. (1999) Regulatory role of p27kip1 in the mouse and human testis. *Endocrinology* 140:1834–1840.
39. Kanatsu-Shinohara M, Takashima S, Shinohara T (2010) Transmission distortion by loss of p21 or p27 cyclin-dependent kinase inhibitors following competitive spermatogonial transplantation. *Proc Natl Acad Sci USA* 107:6210–6215.
40. Kim JK, Diehl JA (2009) Nuclear cyclin D1: An oncogenic driver in human cancer. *J Cell Physiol* 220:292–296.
41. Beumer TL, Roepers-Gajadien HL, Gademan IS, Kal HB, de Rooij DG (2000) Involvement of the D-type cyclins in germ cell proliferation and differentiation in the mouse. *Biol Reprod* 63:1893–1898.
42. Deng X, Ewton DZ, Pawlikowski B, Maimone M, Friedman E (2003) Mirk/dyrk1B is a Rho-induced kinase active in skeletal muscle differentiation. *J Biol Chem* 278: 41347–41354.

OPEN ACCESS Freely available online

PLOS | ONE

Distribution of Artificial Radionuclides in Abandoned Cattle in the Evacuation Zone of the Fukushima Daiichi Nuclear Power Plant

Tomokazu Fukuda[1☯], Yasushi Kino[2☯], Yasuyuki Abe[3], Hideaki Yamashiro[4], Yoshikazu Kuwahara[5], Hidekazu Nihei[2], Yosuke Sano[2], Ayumi Irisawa[2], Tsutomu Shimura[5], Motoi Fukumoto[5], Hisashi Shinoda[6], Yuichi Obata[7], Shin Saigusa[8], Tsutomu Sekine[9], Emiko Isogai[1], Manabu Fukumoto[5]*

1 Graduate School of Agricultural Sciences, Tohoku University, Sendai, Miyagi, Japan, **2** Graduate School of Science, Tohoku University, Sendai, Miyagi, Japan, **3** Graduate School of Science and Engineering, Yamagata University, Tsuruoka, Yamagata, Japan, **4** Faculty of Agriculture, Niigata University, Niigata, Niigata, Japan, **5** Department of Pathology, Institute of Development, Aging and Cancer, Tohoku University, Sendai, Miyagi, Japan, **6** Graduate School of Dentistry, Tohoku University, Sendai, Miyagi, Japan, **7** RIKEN BioResource Center (BRC), Tsukuba, Ibaraki, Japan, **8** National Institute of Radiological Sciences, Chiba, Chiba, Japan, **9** Center for the Advancement of Higher Education, Tohoku University, Sendai, Miyagi, Japan

Abstract

The Fukushima Daiichi Nuclear Power Plant (FNPP) accident released large amounts of radioactive substances into the environment. In order to provide basic information for biokinetics of radionuclides and for dose assessment of internal exposure brought by the FNPP accident, we determined the activity concentration of radionuclides in the organs of 79 cattle within a 20-km radius around the FNPP. In all the specimens examined, deposition of Cesium-134 (^{134}Cs, half-life: 2.065 y) and ^{137}Cs (30.07 y) was observed. Furthermore, organ-specific deposition of radionuclides with relatively short half-lives was detected, such as silver-110m (^{110m}Ag, 249.8 d) in the liver and tellurium-129m (^{129m}Te, 33.6 d) in the kidney. Regression analysis showed a linear correlation between the radiocesium activity concentration in whole peripheral blood (PB) and that in each organ. The resulting slopes were organ dependent with the maximum value of 21.3 being obtained for skeletal muscles ($R^2 = 0.83$, standard error (SE) = 0.76). Thus, the activity concentration of ^{134}Cs and ^{137}Cs in an organ can be estimated from that in PB. The level of radioactive cesium in the organs of fetus and infants were 1.19-fold ($R^2 = 0.62$, SE = 0.12), and 1.51-fold ($R^2 = 0.70$, SE = 0.09) higher than that of the corresponding maternal organ, respectively. Furthermore, radiocesium activity concentration in organs was found to be dependent on the feeding conditions and the geographic location of the cattle. This study is the first to reveal the detailed systemic distribution of radionuclides in cattle attributed to the FNPP accident.

Citation: Fukuda T, Kino Y, Abe Y, Yamashiro H, Kuwahara Y, et al. (2013) Distribution of Artificial Radionuclides in Abandoned Cattle in the Evacuation Zone of the Fukushima Daiichi Nuclear Power Plant. PLoS ONE 8(1): e54312. doi:10.1371/journal.pone.0054312

Editor: Suminori Akiba, Kagoshima University Graduate School of Medical and Dental Sciences, Japan

Received July 7, 2012; **Accepted** December 11, 2012; **Published** January 23, 2013

Funding: This study was supported by an Emergency Budget for the Reconstruction of Northeastern Japan, MEXT, Japan; Discretionary Expense of the President of Tohoku University; National Cancer Center Research and Development Fund, Japan; The Research and Development Projects for Application in Promoting New Policy of Agriculture, Forestry and Fishers, MAFF, Japan; Programme for Promotion of Basic and Applied Researches for Innovations in Bio-oriented Industry, BRAIN, Japan. The funders had no role in study design, data collection and analysis, decision to publish, or preparation of the manuscript.

Competing Interests: The authors have declared that no competing interests exist.

* E-mail: fukumoto@idac.tohoku.ac.jp

☯ These authors contributed equally to this work.

Introduction

The accident at the Fukushima Daiichi Nuclear Power Plant (FNPP) discharged volatile artificial radionuclides such as ^{129m}Te, ^{132}Te, ^{131}I, ^{132}I, ^{133}Xe, ^{134}Cs, ^{136}Cs and ^{137}Cs into the environment [1–5]. The details of the timing and causes of the radioactive releases have been monitored by Tokyo Electric Power Company (TEPCO) (http://www.tepco.co.jp/nu/fukushima-np/f1/index-e.html). The Ministry of Education, Culture, Sports, Science and Technology (MEXT), Japan, and the U.S. Department of Energy (U.S. DOE) examined the airborne dose rate 1 m above the ground surface within 80 km from the FNPP (http://radioactivity.mext.go.jp/en/). In order to assess biological effects of radiation exposure, evaluations of both external and internal exposure are important. While a variety of data pertaining to external exposure are available, only limited data of the internal distribution of radionuclides and their activity are available. Deposits and internal exposure of radionuclides are dependent on the metabolism and biokinetics of radionuclides, which are not fully understood in animals. As of April 22, 2011, the evacuation zone was set to within a 20-km radius surrounding the FNPP, and approximately 3,400 cows, 31,500 pigs, and 630,000 chickens were left behind in this area. On May 12, 2011, the Japanese government ordered Fukushima Prefecture to euthanize the cattle in the evacuation zone. Recently, Calabrese indicated the importance of risk assessment for chronic radiocesium exposure based on the situation at Fukushima in Japan and emphasized the limitation for the assessment of risk from radiocesium intake due to the absence of animal model chronic bioassays [6]. Almost all of the cattle abandoned in the evacuation zone can be recognized

individually by their ear-tag and their individual histories are easily obtainable. We therefore thought that those would be ideal as an animal model for assessing chronic exposure to radionuclides after the FNPP accident. In order to provide basic information for biokinetics of radionuclides and for dose assessment of internal exposure, we evaluated gamma-ray emitting artificial radionuclides in multiple organs of the cattle and analyzed their organ specificity and metabolism.

Results and Discussion

Between August 29 and November 15, 2011, we collected 79 cattle in total, 27 of which were from Minami-soma city located north and 52 from Kawauchi village located southwest of the FNPP. Both places are within the evacuation zone between 10- and 20-km radius of the FNPP. The cattle included 63 adult females (3 of which were pregnant), 10 male calves, and 3 female calves. The age of the cattle without the ear-tag was estimated by its height and body size. We classified the cattle as infant if it was younger than 6 months old.

Typical gamma-ray spectra obtained from muscle, liver, and kidney are shown in Figure S1. In these spectra, either of photopeaks from ^{134}Cs, ^{137}Cs, ^{110m}Ag, and ^{129m}Te was observed. In the control animals, which were housed in Hokkaido Prefecture (northern edge of Japan, 630 km from FNPP), we could not detect any photopeaks of ^{134}Cs, ^{137}Cs, ^{110m}Ag, and ^{129m}Te (data not shown). We also determined the limit of detection based on the background measurement (see "Materials and Methods"). From these data, we concluded that the detected radionuclides, such as ^{134}Cs, ^{137}Cs, ^{110m}Ag, and ^{129m}Te, in the abandoned cattle were attributable to environmental contamination by the nuclear fallout from the FNPP accident.

Based on the count rate from each cattle organ, we calculated the concentration of these radionuclides, as listed in Table 1. All the measurements were decay-corrected to the day of major release, March 15, 2011 (see the section on decay correction in Materials and Methods). All specimens including peripheral blood (PB) obtained from abandoned cattle showed deposition of two radionuclides, ^{134}Cs and ^{137}Cs. The measured radioactivity of ^{134}Cs was similar to that of ^{137}Cs after decay correction in all samples examined. Therefore, both isotopes of radiocesium are hereafter represented by ^{137}Cs. Muscle tissues showed the highest deposition of ^{137}Cs and no statistical difference of ^{137}Cs activity concentration was observed among three representative positions of the cattle muscle (*Longissimus*, *Biceps femoris*, and *Masseter* muscle). We thus classified these three muscles into one category, "skeletal muscle," in the subsequent regression analysis between PB and organs.

In the liver (100%: 47/47 animals) and PB (9.8%: 5/51 animals), ^{110m}Ag (half-life: 249.8 d) was detected (Table 1). Furthermore, kidney (62%: 18/29 animals) showed the deposition of ^{129m}Te, despite its short half-life (33.6 d), whereas other specimens including PB did not.

Regression analysis revealed linear correlations of ^{137}Cs activity concentration between PB and organs. The slope was dependent on each organ examined (Figure 1), indicating that radiocesium activity concentrations in the organs can be estimated from the blood levels. The activity concentration level of ^{137}Cs in the skeletal muscle was the highest among all of the organs examined and was 21.3-fold greater (standard error (SE) = 0.76) than that of PB. The difference of the regression slopes between the skeletal muscle and other organs was significant (t-test, Table S1). Interestingly, ^{137}Cs activity concentration in the heart was significantly lower than that in skeletal muscles despite the fact that the heart is composed of striated muscle cells.

Cattle were divided into 3 groups in accordance with the plot in which they were caught. Plots 1 and 3 were in Minami-soma city located to the north and plot 2 in Kawauchi village located to the southwest of the FNPP, respectively. Cattle in Plot 1 were kept in a stall barn after the FNPP accident, and they were fed with radionuclide-free pasture grass and supplied with radiation contaminated rainwater until sacrifice. Cattle in Plots 2 and 3 were unleashed and were freely allowed to graze on contaminated grass after the accident. The profile of rdiocesium activity concentration could be divided into 3 groups in accordance with the Plot where the cattle were caught (Figure 1 and Table S2). Although Plots 1 and 3 were the same city, the feeding conditions were different. The level of ^{137}Cs activity concentration in soil samples between Plot 2 and Plot 3 was not so different (Table S3) and was also reportedly quite similar [7]. However, ^{137}Cs activity concentration in PB of cattle in Plot 3 was the highest and that in Plot 1 was the lowest in this study (comparison of each group, $p<0.01$, t-test). These indicate that the activity concentration of internally deposited radionuclides is largely influenced by feeding conditions as well as geographic conditions of the cattle farm.

The transfer of radionuclides from mother to fetus is one of the major concerns of exposure to internal radiation. As mentioned above, we had collected 3 pregnant cows. The comparison between radiocesium activity concentration in the fetus and the mother is shown in Figure 2A. Most symbols lay on the upper part of the dashed equality line (fetus side). The regression analysis of all tested organs showed that the activity concentration of cesium was 1.19 times higher ($R^2 = 0.62$, SE = 0.12) in fetal organs than in the corresponding maternal organs. Cesium is considered to transfer freely between mother and fetus and is assumed to be uniformly distributed throughout all the tissues of the fetus [8]. These observations indicate that radiocesium is more concentrated in the fetus than in the mother. Although Silver and Tellurium are transplacental [9–11], neither ^{110m}Ag nor ^{129m}Te was detectable in the fetal organs examined, indicating that these radionuclides were efficiently captured by the mother's organs and were not delivered to the fetus. In order to understand fetal biokinetics of each radionuclide we tried to collect PB from the fetus. However, we could not obtain sufficient quantities to enable the measurement of radioactivity.

Before the cattle were euthanized, we noticed 3 mother and infant pairs in Plot 2. We confirmed that these infants were born after the FNPP accident and that they were being weaned at the time. As shown in Figure 2B, most of the points lie on the upper side of the dashed equality line (infant side). The regression analysis showed that radiocesium activity concentration was 1.51 times higher in the infant organs than in the corresponding maternal organs ($R^2 = 0.70$, SE = 0.09). Therefore, we concluded that the deposition of ^{137}Cs in infant organs is correlated with that in the corresponding maternal organs but is higher than that in maternal ones. Shorter half-lives of retention are adopted for infants and children than for adults [12]. Inaba *et al.* mentioned that water and electrolyte metabolism should differ considerably between newborn and adult, and that potassium contents of the feeding might affect the radiocesium activity concentration [13]. We do not have any data regarding the proportion attributed to milk and grass which the infants were taking at the time of the sacrifice.

In our data, the thyroid showed lower ^{137}Cs deposition compared with other visceral organs (Figures 1 and 2B). Bandazhevsky previously reported that the highest accumulation of radiocesium was found in the endocrine glands, in particular,

Table 1. Activity concentration of ^{134}Cs, ^{137}Cs, ^{110m}Ag and ^{129m}Te in cattle organs and peripheral blood.

	Cs-134 (Bq/kg)[a]			Cs-137 (Bq/kg)[a]			Ag-110m (Bq/kg)[a]			Te-129m (Bq/kg)[a]		
	mean ± SD[b]		num[c]	mean ± SD[b]		num[c]	mean ± SD[b]		num[c]	mean ± SD[b]		num[c]
Longissimus muscle	592	±398	48	611	±416	48		ND[d]			ND	
Biceps femoris muscle	637	±420	38	665	±442	38		ND			ND	
Masseter muscle	579	±359	19	606	±373	19		ND			ND	
Neck muscle	549	±300	6	568	±327	6		ND			ND	
Diaphragm	272	±206	12	289	±233	12		ND			ND	
Tongue	584	±310	17	619	±334	17		ND			ND	
Heart	301	±176	30	311	±187	30		ND			ND	
Liver	198	±145	47	207	±154	47	177	±176	47/47[e]		ND	
Kidney	344	±249	29	361	±264	29		ND		7,000	±6,000	18/29[e]
Lung	272	±186	35	275	±183	35		ND			ND	
Spleen	182	±98	20	190	±106	20		ND			ND	
Thyroid gland	200	±231	8	192	±207	8		ND			ND	
Submandibular gland	162	±101	11	178	±114	11		ND			ND	
Mammary gland	54	±60	3	54	±55	3		ND			ND	
Uterus	128	±114	6	143	±125	6		ND			ND	
Urinary bladder	186	±80	5	210	±94	5		ND			ND	
Brain	119	±36	3	123	±38	3		ND			ND	
Eye	103	±55	11	110	±62	11		ND			ND	
Blood	24	±20	51	25	±19	51	5.2	±3.7	5/51[e]		ND	

[a]Decay correction was made to the day major release of radionuclides, March 15, 2011.
[b]SD: the standard deviation.
[c]num: the number of the samples positive for the deposition of radionucleides.
[d]ND: not detectable.
[e]The Number of positive samples/the number of tested samples. All the samples were positive for ^{134}Cs and ^{137}Cs.
doi:10.1371/journal.pone.0054312.t001

the thyroid, in humans [14]. Although we need to consider the species difference between humans and cattle, radiocesium is suggested to have little impact on thyroid carcinogenesis.

Chronic inflammation and the development of proliferative atypical cells of the bladder uroepithelium in people living in ^{137}Cs-contaminated areas in Ukraine have previously been reported [15]. The urinary bladder showed relatively high ^{137}Cs accumulation in this study (Figure 1). In our observation, so far, we could not find any abnormalities at the gloss appearance level in the bladder.

Radioactive ^{110m}Ag is not a fission product but is formed by the neutron capture of stable ^{109}Ag. We detected ^{110m}Ag in the liver of all of the cattle except for fetuses examined (Table 1 and Figure 3A). The ratio of deposited radioactivity concentration of ^{110m}Ag to ^{137}Cs in the soil of Plot 2 and Plot 3 was lower than 0.5% and that in the grass of Plot 3 was lower than 5% (Table S3). The value in the soil was consistent with the distribution map of radiation doses by MEXT (http://radioactivity.mext.go.jp/old/en/1750/2011/10/1750_1031e_2.pdf) (MEXT Dose Map) as of June 14, 2011. In the current study, ^{110m}Ag activity concentration in the liver did not show Plot dependent difference or association with ^{137}Cs activity concentration (Figure 3A). Both the human evidence and the animal studies indicate substantial deposition of silver in the liver but the retention rate is influenced by the route of intake [12]. It is reported that the liver deposition of ^{110m}Ag in sheep and its transfer coefficient to the liver was higher than that of ^{137}Cs in the Chernobyl nuclear accident [16]. These data indicate that the transfer coefficient of ^{110m}Ag to the liver is higher than that of ^{137}Cs. Furthermore, post-mortem data on the distribution of ^{110m}Ag in a patient 195 days after injection showed the highest uptake in the liver (40%) among all organs [17]. There was no relationship between the activity concentration of ^{110m}Ag in PB and in the liver (Figure 3B). Danscher *et al.* reported that silver predominantly accumulates in lysosome-associated tissues, such as lymph nodes, liver, kidneys and the central nervous system after silver administration in rats and mice. Furthermore, they showed the intense accumulation of silver in Kupper cells of the liver [18]. From these cumulative data and this study, we concluded that the liver is the primary target organ for ^{110m}Ag deposition.

We clearly detected the radioactivity of ^{129m}Te in the cattle kidney (Table 1), although the measurement was performed 7 months after the FNPP accident. We concluded that the kidney is the target organ of ^{129m}Te deposition, based on its relatively short half-life (^{129m}Te, 33.6 d). The activity concentration of ^{129m}Te was mainly classified into two groups: Plots 2 and 3 (Figure 3C). The ratio of $^{129m}Te/^{137}Cs$ activity concentration in the kidney of some cattle from Plot 2 was higher than that from Plot 3. As of March 15, the ratio of soil activity concentration of ^{129m}Te to ^{137}Cs was 0.34 in Plot 2 and 1.41 in Plot 3, respectively [7]. This contradiction needs further investigation.

After the FNPP accident, a large amount of ^{132}Te was released into the environment. At first a higher activity concentration of ^{132}Te than ^{129m}Te was detected in the soil of the evacuation zone [7]. The deposition of ^{129m}Te in the kidney suggests that radioactive ^{132}Te also accumulated in the kidney shortly after the FNPP accident. The half-life of ^{132}Te is 3.2 days and its decay product is radioactive ^{132}I, which is thyroid tropic. A previous study reported that radioactive tellurium that is orally adminis-

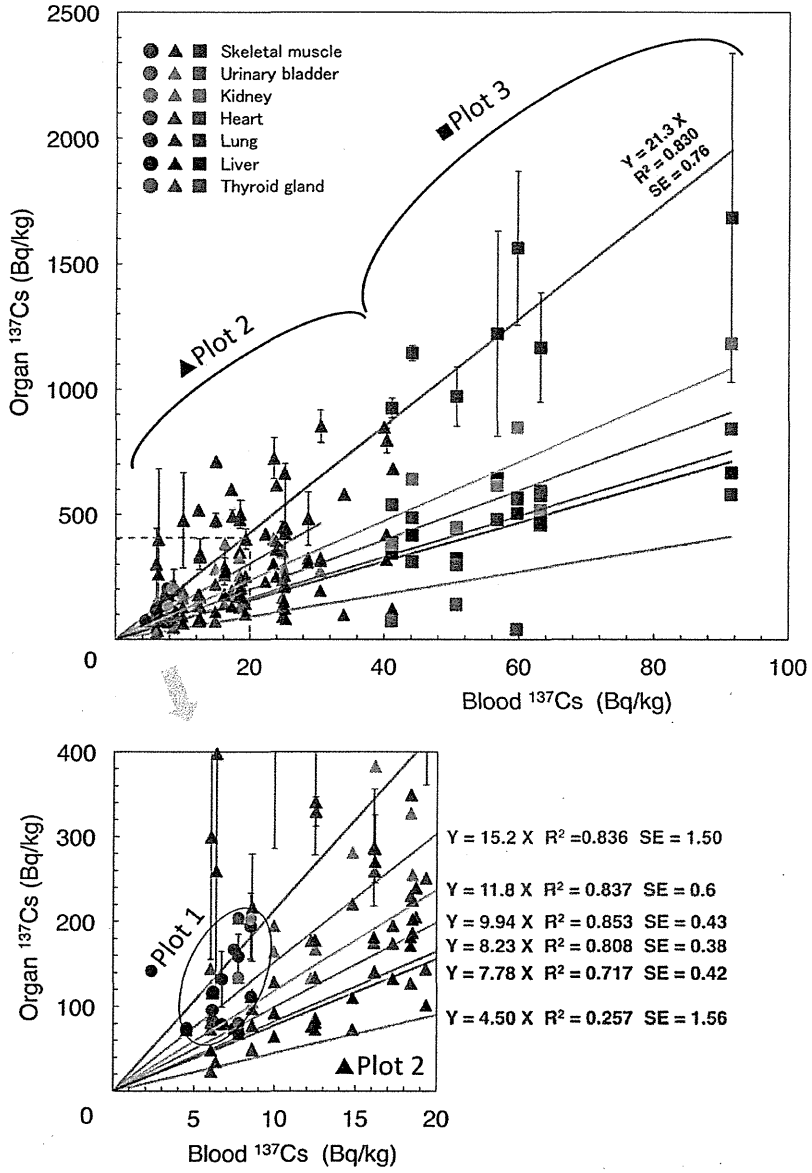

Figure 1. Correlation of ^{137}Cs activity concentration between peripheral blood (PB) and organs. Cattle were captured in Plots 1(circle), 2 (triangle), and 3 (square). Cattle from the same plot were enclosed by black marking. Inset: Cattle whose ^{137}Cs radiation concentration in PB was lower than 20 Bq/kg. All those from Plot 1 and part of Plot 2 were included.
doi:10.1371/journal.pone.0054312.g001

tered to cows concentrates in the thyroid more than in most other tissues [19]. These results suggest that we need to pay more attention to ^{132}Te as well as ^{131}I in assessing health risk to the thyroid.

Currently, we are further collecting tissues from animals, including cattle, in the evacuation zone in order to construct a tissue bank which represents a variety of species. As the first stage, we are going to make dose assessments of deposited radionuclides in animals. Microscopic examinations of necropsied animals are also underway to find lesions that could be directly attributed to the effect of ionizing radiation. Our study is the first report on organ-specific deposits of various gamma-ray emitting radionuclides in cattle after the FNPP accident, and should contribute to improvement in public health and radiation safety.

Materials and Methods

Ethics

This study is one of the national projects associated with the Great East Japan Earthquake and has been entirely endorsed and supported by the Japanese government through the Ministry of Education, Culture, Sports, Science and Technology, Japan. The Japanese government ordered Fukushima Prefecture to euthanize cattle in the evacuation zone on May 12, 2011 to prevent radiocontaminated beef products entering the human food chain. We

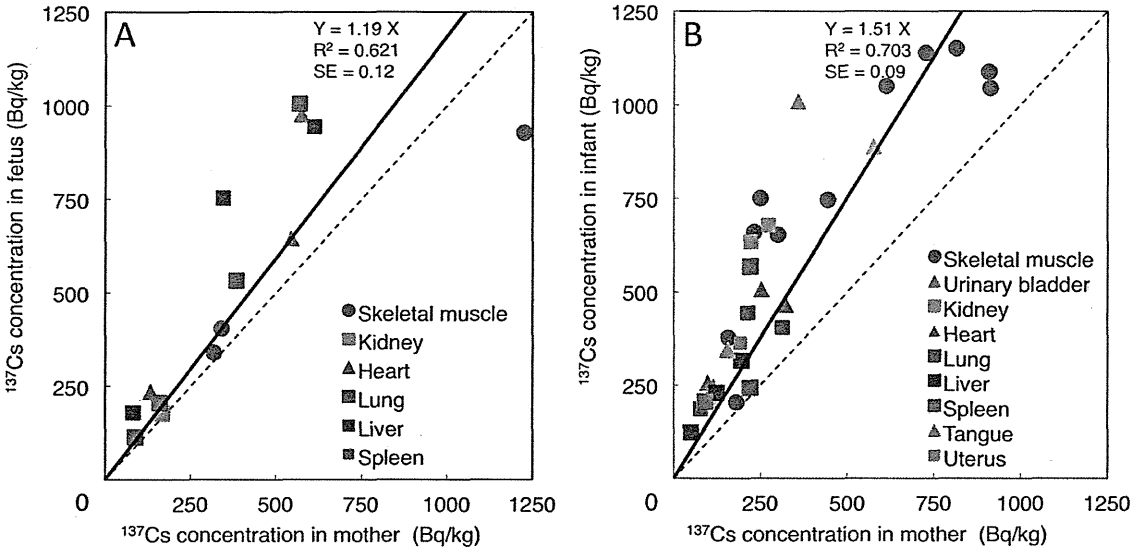

Figure 2. Comparison of ^{137}Cs activity concentration between mother and offspring. A. Organ ^{137}Cs activity concentration between 3 pairs of mother and her fetus. **B.** Organ ^{137}Cs activity concentration between 3 pairs of mother and her child. The dashed line indicates the slope at which ^{137}Cs activity concentration in organs is equal between mothers and their corresponding offsprings. Points above this line indicate that offspring ^{137}Cs activity concentration in an organ was higher than that of the mother. The bold line is the regression line obtained from all organs.
doi:10.1371/journal.pone.0054312.g002

collected organs and tissues from the euthanized cattle by the combined unit of veterinary doctors belonging to the Livestock Hygiene Service Center (LHSC) of Fukushima Prefecture and those belonging to the Ministry of Agriculture, Forestry and Fisheries, Japan. Cattle were sacrificed by these veterinarians by the following method according to the Regulation for Animal Experiments and Related Activities at Tohoku University (Regulation No 122) briefly described as below. The owner of each cattle was identified by the ear tag of the cattle and informed consent from the owner was obtained by the veterinary doctors of Fukushima Prefecture. The procedure of euthanasia was entirely carried out by the veterinary doctors of LHSC. The cattle used as negative control for radioactive substances were used for practical training of anatomy for students at Rakuno Gakuen University, Hokkaido, Japan. Use of the cattle for this study was approved by the Ethics Committee for Animal Experiments of Rakuno Gakuen University. These cattle were sacrificed by exanguination from the jugular vein in their unconscious state by a pentobarbital overdose via intramuscular injection of hypnotics (Xylazine hydrochloride, 0.2 mg/kg), then PB was collected from the jugular vein, after which Pentobarbital (2 mg/kg) and Suxamethonium were injected.

Collection of specimens

Between August 29 and November 15, 2011, we obtained PB and organ samples from cattle collected in the evacuation zone of the FNPP. All cattle born before the FNPP accident had the ear tag with an individually unique 10-digit number for identification, however, those born after the FNPP accident did not. After tranquilization by intramuscular injection of hypnotics (Xylazine hydrochloride, 0.2 mg/kg), PB was collected from the jugular vein and then Pentobarbital (2 mg/kg) and Suxamethonium chloride (1 mg/kg) were injected. We collected tissues within 1 hr after veterinary doctors euthanized the cattle. Because dissection was carried out in an open field with limited time being spent in the evacuation zone, the number of organs extirpated differed among individual cattle, for example, only blood samples and a single muscle sample could be obtained from some cattle. PB and organ samples were preserved at −20°C until radioactivity was measured. The number of organ samples analyzed is shown in Table 1. Soil and grass samples were collected at the place where the cattle were caught. Soil samples were taken in a square 30×30 cm from the surface to the depth of 1 cm. Radioactivity concentration was calculated into kBq/m^2 by [measured radiation concentration (Bq/kg)]×[measured density (kg/m^3)]×[depth (0.01 m)]. We carefully selected grasses with bite marks of cattle if possible and radioactivity concentration was calculated into Bq/wet weight.

Collection of control specimens

In Hokkaido Prefecture (northern edge of Japan, 630 km from FNPP), we collected samples from 2 male and 1 female cows housed in this area that were around 17 days of age. Furthermore, their mothers were supplied with radionuclide-free feed. Organs dissected from these cattle were used as negative control, which are free for radionuclides from FNPP. After the cattle were euthanized, the same cattle organs as listed in the previous section were dissected. The radionuclides in the control organs were measured by the same method as that for the abandoned cattle, as described in the next section.

Measurements of radioactivity

The radioactivity of the samples was determined by gamma-ray spectrometry using three HPGe detectors (Ortec Co., USA). The measurement time varied from 3,600 to 200,000 s depending on the radioactivity of the samples. The efficiency was determined by measuring mixed sources of ^{152}Eu and ^{137}Cs. An aliquot (200 ml) of the mixed source was diluted with appropriate amounts of water, and superabsorbent polymer was added to the mixture to make a gel standard source. The gel source was used as a mock sample to imitate tissue samples, and several types of gel sources were prepared to cover a weight range from 0.5 to 110 g. Aqueous

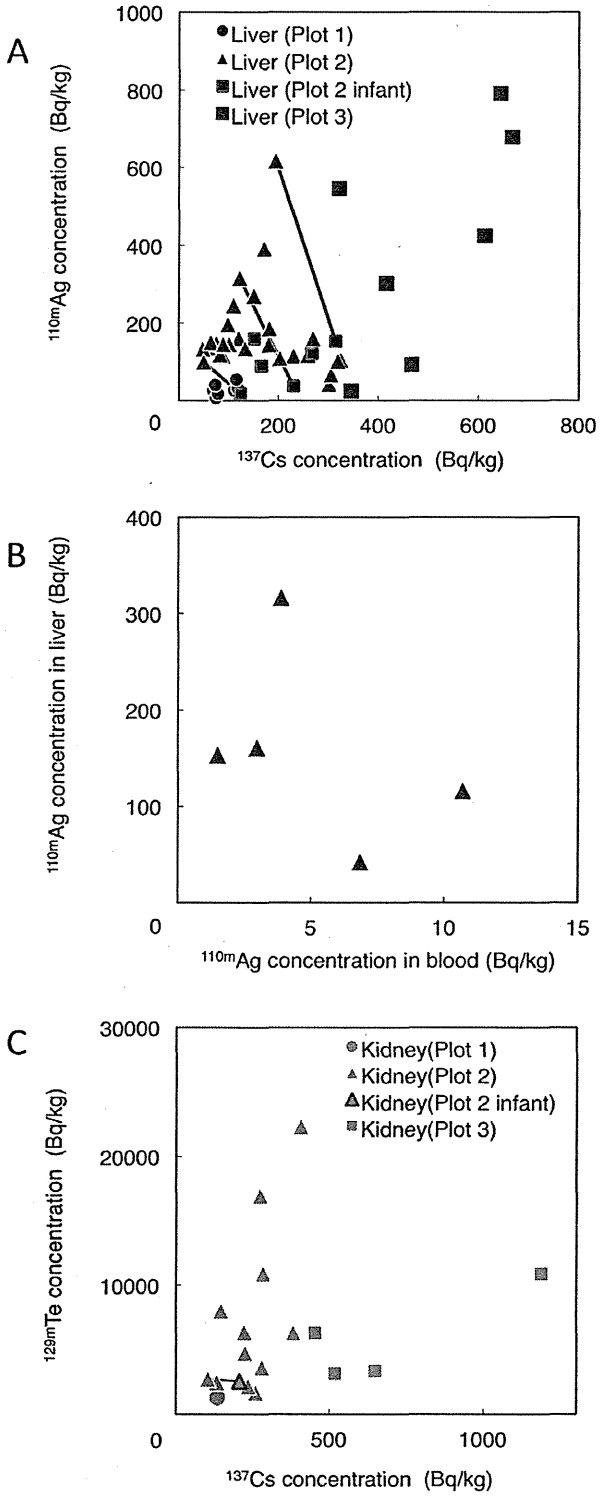

Figure 3. Activity concentration of ^{110m}Ag and ^{129m}Te. A. The activity concentration of ^{137}Cs and ^{110m}Ag in the liver. **B.** The activity concentration of ^{110m}Ag in peripheral blood and in the liver. Radioactivity form ^{110m}Ag was detectable in 5 out of 51 cattle. **C.** Activity concentrations of ^{137}Cs and ^{129m}Te in the kidney. Mother-child relationship is indicated by green lines.
doi:10.1371/journal.pone.0054312.g003

solutions of ^{152}Eu and ^{137}Cs were used to determine the efficiency for liquid samples such as PB. Samples were homogenized and sealed in polyethylene vials (1–100 ml) depending on their mass. A nuclide was identified when its characteristic photopeaks of greater than 3σ above the baseline were observed in the spectrum. In addition, we determined the radioactivity detection limit from the background level: it was found to be 0.1–0.2 Bq/kg for organs from which we could obtain sufficient quantities of samples to fill a 100-ml vial and 0.7–0.8 Bq/kg for relatively tiny organs (less than 10 g in weight), such as the thyroid gland.

Decay correction

Presenting radioactivity measured as a (Bq), the activity after the decay correction is given by a_0 (Bq). We can obtain the number of days, t from March 15, 2011 to the date of the measurement. The half-life, T is 250 days for ^{110m}Ag, 34 days for ^{129m}Te, 754 days for ^{134} Cs and 11,016 days for ^{137}Cs.

The activity after the decay correction is given by:

$$a_0 = a \times 2^{\frac{t}{T}}.$$

Statistic analysis

Linear regression analysis was performed to determine the relationship of two variables and to evaluate the regression line and standard error. The difference between the regression slopes of two groups was found to be significant in case $p<0.05$ with the standard t-test.

Supporting Information

Figure S1 Representative detected photopeaks for internal radionuclides in organs of a cattle. A. Both peaks form ^{134}Cs and ^{137}Cs are highest in the muscle among organs meaured. **B.** Characteristic peaks to ^{110m}Ag are observed in the liver but not in the muscle or the kidney. **C.** A peak from ^{129m}Te is obsereved in the kidney but not in the muscle or the liver.
(TIF)

Table S1 P values for null hypothesis test between regression slopes of two different organs determined (t-test). * The value of slopes: Skeletal muscle>Urinary bladder>''' Kidney>Heart>Lung>Liver>Thyroid gland
(TIFF)

Table S2 Concentration of 134Cs and 137Cs in cattle organs. [a] Skeltal muscles: Longissimus muscle, Biceps femoris muscle and Masseter muscle combined. [b]SD: Standard deviation. [c] num: the number of the samples positive for the deposition of radionucleides.
(TIFF)

Table S3 Radioactivity concentration in the soil (kBq/m2) and in the grass (Bq/kg). [a]JPG: Japanese pampas grass. [a]ND: not detectable.
(TIFF)

Acknowledgments

We are grateful to those who were involved in this study, especailly Dr. Masahiro Hotta, Dr. Hirokazu Tamura (Graduate School of Science, Tohoku University) for their technical help and helpful discussion. We also thank to Mr. Tetsuya Amanuma, Mr. Kazuya Inoue, Ms. Ai Kurihara, Mr. Naoto Noma, Mr. Toshiyuki Oikawa, Mr. Yasuyuki Ochiai, Ms. Yui Sano, Mr. Shintaro Takahashi (Department of Pathology, Institute of